RESEARCH ARTICLE-CIVIL ENGINEERING

Dynamic Response of a Structure Exposed to Earthquake Rotational Components and Soil–Structure Interaction Effects

Osman Akyürek[1] · **Bilal Baran**[1]

Abstract

The effects of rotational (torsional and rocking) components of an earthquake are often neglected in dynamic analyses, as most modern codes only provide horizontal and vertical elastic spectral curves. However, neglecting these components can lead to the unrealistic results, especially when considering soil–structure interaction effects. Incorporating soil–structure interaction (SSI) significantly changes the behavior of structures, affecting their modes, shapes, and mass participation ratios. This emphasizes the importance of rotational modes and their impact on structural responses, including lateral and rotational displacement, velocity, and acceleration. The study aims to examine the effects of SSI while considering rotational earthquake motions on structural responses. Therefore, the Benchmark structure was placed on different soil types (very soft, soft, medium, and dense soil), and time history analyses were conducted. The results showed that rotational components significantly affect dynamic characteristics and structural performance indexes such as the fundamental period, base shear, inter-story drift ratios, maximum floor acceleration, and input energy. Taking rotational components into account is necessary for more accurate results, especially when the foundation is on soil with a shear velocity of less than 100 m/s.

Keywords Soil–structure interaction · Rocking component · Torsional component · Isolation effect · Directivity effect · Input energy · Benchmark building

List of symbols

A_0	Cross-sectional area of the footing
AGM	Acceleration gradient method
BS	Base shear
C	Damping coefficient
c_h	Equivalent horizontal damping coefficient
c_r	Equivalent rocking damping coefficient
c_t	Equivalent torsional damping coefficient
c_v	Equivalent vertical damping coefficient
DE	Directivity effects
E_{ir}	Input energy
FA	Floor accelerations
FEMA	Federal Emergency Management Agency
G	Shear modulus
GM	Geodesy method
I_0	Mass moment of inertia of the foundation system
IDR	Inter-story drift ratio
ISE	Isolation effect
k	Stiffness
k_h	Equivalent horizontal stiffness
k_r	Equivalent rocking stiffness
k_t	Equivalent torsional stiffness
k_v	Equivalent vertical stiffness
L_x	Total length of the building in the x-directions
L_y	Total length of the building in the y-directions
M	Mass moment of inertia of the entire structure
m_0	Mass of the foundation system
$\max\lvert Q_x\rvert$	Maximum absolute value in the rotational data in the x-direction of the earthquake
$\max\lvert Q_y\rvert$	Maximum absolute value in the rotational data in the y-direction of the earthquake
$\max\lvert Q_z\rvert$	Maximum absolute value in the rotational data in the z-direction of the earthquake
$\max\lvert T_x\rvert$	Maximum absolute value of the translational components of the earthquake in the x-direction

✉ Osman Akyürek
    oakyurek@nevsehir.edu.tr

    Bilal Baran
    bilalbaran@nevsehir.edu.tr

1   Department of Civil Engineering, Nevsehir Haci Bektasi Veli University, Nevsehir, Turkey

🖄 Springer

max$	T_y	$	Maximum absolute value of the translational components of the earthquake in the y-direction
max$	T_z	$	Maximum absolute value of the translational components of the earthquake in the z-direction
MSP	Multi-station procedure
$\varnothing$	Rocking angles
θ	Torsional angles
r_{0h}	Equivalent horizontal radius of the foundation
r_{0r}	Equivalent rocking radius of the foundation
r_{0t}	Equivalent torsional radius of the foundation
r_{0v}	Equivalent vertical radius of the foundation
RSA	Response spectrum analysis
r_x	Radius of rotation in the x-direction
r_y	Radius of rotation in the y-direction
SDM	Surface distribution method
SDOF	Single degree of freedom
SF	Scale factors
SF_r	Rocking scale factor
SF_t	Torsional scale factor
SF_x	Rotation scale factor around the x-direction
SF_y	Rotation scale factor around the y-direction
SF_z	Rotation scale factor around the z-direction
SSI	Soil–structure interaction
SSP	Single-station procedure
THA	Time history analysis
u_h	Lateral structural responses due to the horizontal components of the ground motion
u_r	Lateral structural responses due to the rocking components of the ground motion
u_s	Lateral response of the structure
u_t	Lateral structural responses due to the torsional components of the ground motion
V_p	Dilatational-wave velocity
V_s	Shear wave velocity
γ	Coefficients for dimensional
ρ	Density
υ	Poisson ratio of the site soil

1 Introduction

A ground motion is composed of three translational components in three directions (x-, y-, and z-directions) and three rotational components around three directions (x-, y-, and z-around), see Fig. 1. Today, the dynamic analyses of residential structures are made under earthquake loading using only the translational components of the earthquake; however, there are special conditions of inclusion of rocking effects that need to be addressed that is stated in Eurocode 8, Part 6 [1] for special structures like water tower, and nuclear plants. Although vertical and horizontal elastic spectrum curves are
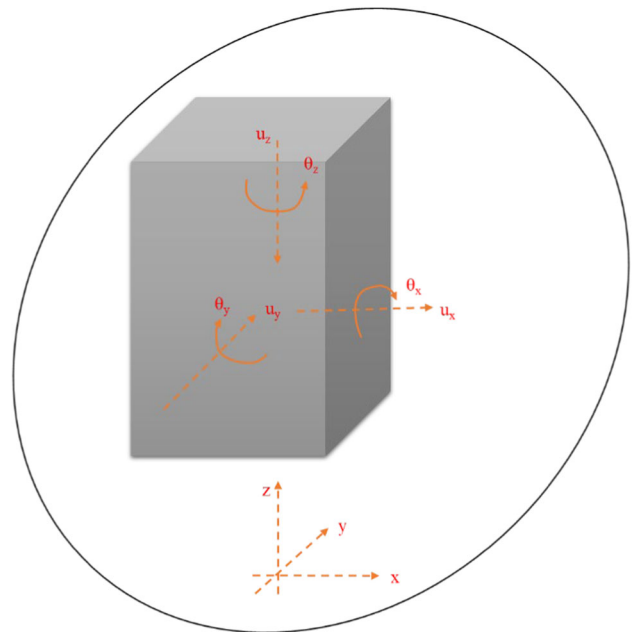
Fig. 1 Under an earthquake loading, a schematic view of a civil structure in horizontal and vertical translational responses and rotational responses around three orthogonal directions [4]

given in the current modern code like ASCE 7-22 [2] and TBDY-2018 [3], there is no spectral information about the rocking and torsional components of the earthquake which are often neglected when considering earthquake effects. However, for buildings that are torsional irregular, high-rise, or constructed on lower soil classes, these components become even more critical.

Earthquakes are inevitable facts of life and most regions of our country (Türkiye) are under this danger. Especially in earthquake-prone regions, building stocks are exposed to serious earthquakes very often. For this reason, earthquake-resistant and performance-based design becomes important for the safety and security of society [5, 6]. For a detailed seismic analysis of a structure, it is necessary to perform a dynamic analysis using all components of the earthquake. For this purpose, both translational (horizontal and vertical) and rotational (rocking and torsional) components of the earthquake should be applied simultaneously to the structure, as seen in Fig. 1. In addition, the effects of the rotational components of the earthquake have led to the assumption that those components do not significantly affect the seismic behavior of the structure, due to observations made in low-rise buildings. Therefore, the effect of these components on the earthquake performance of the structure is thought to be negligible, which led to those components not being used in earthquake simulations. However, this assumption does not include high-rise buildings, buildings with torsional irregularities and soil–structure interaction effects. In modern earthquake codes like Eurocode 8, Part 6, in addition to

the elastic spectrum curves for the translational directions, some additional conditions are presented for the rotational components as a special condition.

Many researchers [7–11] in earthquake engineering and seismology have been working to obtain records of the rotational components of earthquakes, especially for the past decade. Although special accelerometers can now record the rotational components of earthquakes in the field, it is also possible to derive these components using saved translational records. Takeo [12] used to record rotational motions of earthquakes by means of a gyro-sensor with a combination of inertial angular displacement sensors throughout a few earthquakes in Japan. Teisseyre et al. [13] were able to compute them by signals from a series of seismographs. Further developments in rotational seismology related to instrumentation, theory, and observations are available for the present studies [14–16]. For computing the rotational components, economical sensors based on electrochemical magneto hydrodynamic technology have also been used [17, 18]. There are also various procedures for deriving reflexive time series from translation records. One of these is the single-station procedure (SSP) [11, 19]. They used SSP to derive rotational components based on their study. Expanding the SSP method involves incorporating data collected by a group of closely situated, spatially dispersed stations. The approach (multi-station procedure (MSP)) can yield valuable insights and enhance the accuracy of the findings [20]. Spudich and Fletcher [21] developed the MSP method and introduced the geodesy method (GM). To alleviate the limitations of the GM method, the acceleration gradient method (AGM) was proposed by Basu et al. [22]. By this method, they obtained the earthquake's rotational components by using its three translational components via a dense array of sensors recording at surface stations. However, the AGM method was not able to extract frequency content above its limitation. The frequency limitation decreases when the physical size of the array increases. This inadequacy of AGM was developed as an alternative technique called the surface distribution method (SDM) by Basu et al. [23].

Jomen et al. [24] investigated the rotational effect of the earthquake theoretically and experimentally by applying the horizontal component of the earthquake to the uneven structure foundation. In their experiment, they observed that the vibration in the horizontal direction is the factor that creates the rotational motion components of the earthquake, and the vertical vibration is the strengthening factor of the rotational components of the earthquake. Vaseva et al. [25], on the other hand, used the tower, which is a slender structure, in their studies. They analyzed this structure by using seismic data (spectrum curves) and the modal analysis method given in the Eurocode 8 regulation. As a result, they drew attention to the fact that the rotational components of the earthquake are caused by the earthquake Rayleigh and Love waves and are natural components of the earthquake. These components should be taken into account in the calculations, especially in high-rise buildings, otherwise, the effects of the earthquake may be underestimated in the structures. In addition to these findings, they suggested that the spectrum curves given in the modern earthquake codes should be updated by considering the rotation effect. Similarly, Pnevmatikos et al. [26] examined the reactions of a regular and irregular steel structure in a ten-story plan under the influence of all components of the earthquake and observed similar results.

In this study, dynamic responses of the Benchmark building under the influence of all components of an earthquake including both the rocking and rotational components, as well as the soil–structure interaction effect are studied. For this reason, the Benchmark building is first exposed to the horizontal and vertical components (x-; y-, and z-) of the El Centro earthquake with and without torsional and rocking components. The structure is then placed on the ground with different soil types; very soft, soft, medium, and hard soil, to see the effect of the rocking and torsional components of the earthquake and the effect of soil–structure interaction on the dynamic behavior of the structure. In addition to that, to take the critical loading direction into account, scale factors are proposed, and the rotational components of the earthquake are enlarged with positive and negative scale factors to create different loading situations. Finally, modal linear time history analysis on three-dimensional finite element model of the structure is made employing the SAP2000 structural software. The results indicate that incorporating soil–structure interaction effects in the analysis enhances the significance of rotational modes (rocking and torsional) and their substantial contribution to total responses, including lateral and rotational displacements, velocity, and acceleration for each floor. It is evident that compared to the fixed-based model, rotational modes become more dominant, especially when excited by earthquake rotational components, and their effects become even more critical in structural responses. The unique aspect of this study is to examine the SSI effects while incorporating rotational earthquake motions on structural responses. Consequently, the rotational and rocking components significantly influence the dominant period of the structure, the base shear force, inter-story drift ratios, maximum acceleration, spectral acceleration, and input energy. In short, it is seen in the analysis results that it should be taken into account the rocking and torsional components as well as the horizontal components of the earthquake to reach a more realistic result and to further improve the structure safety conditions when performing the dynamic analysis of the structure against earthquake.

Table 1 Structural components (section profiles) used in the Benchmark building

Story no	Height (m)	Exterior columns	Interior columns	Beams
1	5.49	W14 × 370	W14 × 500	W36 × 160
2	3.96	W14 × 370	W14 × 500	W36 × 160
3	3.96	W14 × 370	W14 × 455	W36 × 135
4	3.96	W14 × 370	W14 × 455	W36 × 135
5	3.96	W14 × 283	W14 × 370	W36 × 135
6	3.96	W14 × 283	W14 × 370	W36 × 135
7	3.96	W14 × 257	W14 × 283	W30 × 99
8	3.96	W14 × 257	W14 × 283	W27 × 84
9	3.96	W14 × 233	W14 × 257	W24 × 68

2 Overview of Model Building

As part of the SAC project, a 9-story steel structure located in California, USA, was chosen for analysis [27]. Constructed by Brandow & Johnston Associates, this building is intentionally chosen for its ability to represent the mid-rise general building stock of Türkiye. The structure met all requirements of the earthquake code and was named a Benchmark building. The selection of this building is also intended to provide a wider range of comparisons for other researchers. The foundation columns were fixed in the foundation. All columns were constructed using 345 MPa steel, while the beams and composite floors were made of 245 MPa steel. The structure features wide-flange (W-) sections for both the beams and columns, as outlined in Table 1.

The building is comprised of a total of 5 spans in both orthogonal directions, with each span having a length of 9.15 m. The moment-resisting frame systems are symmetrically positioned along the outer axes of the structural plan, as depicted in Fig. 2a. This design ensures that the structure does not possess any inherent eccentricity. Furthermore, the column's placement on the floor plan can be found in Fig. 2b. The elevation view of 6–6 axis is also presented in Fig. 2c. Internal columns and beams were simply connected and therefore do not have moment-carrying capabilities. Rigid diaphragms were assigned to all floor levels of the composite floors to make the structure behave cohesively. The diaphragms allowed load-bearing members such as columns and beams to share earthquake loads.

2.1 Modal Verification for the Model Building

According to Ohtori et al. [28], the masses for each floor assuming collected at the center of gravity are 9.65×10^5 kg for the basement, 1.01×10^6 kg for the first floor, 9.89×10^5 kg from the second through eighth floors, and 1.07×10^6 kg for the last floor. The total building mass is given as 9.00×10^6 kg. These loads given for each floor were assigned as the dead load distributed on the floors with the help of

the SAP2000 software and taken as the mass source. The structure in this study is taken as a reference to model the 3D version of the 9-story Benchmark building. However, in their study, they only used a lumped mass model instead of a 3D model. Therefore, they only have dynamic properties such as the period for one (x-) direction. In this study, the Benchmark building is designed as a 3D FEM model. Mesh area using a general divide tool based on points and lines in the meshing group is used with a maximum size of the divided object (2 m^2) for slab elements. For beam and column elements, an auto mesh frame is used. Thanks to 3D modeling, the first nine frequency modes were obtained and tabulated in Table 2.

Table 2 shows that the first mode of the 3D model is 0.415 Hz, which is very similar to Ohtori et al.'s [28] findings. Furthermore, the second and third modes are close enough to the referenced study, with differences of less than 0.1%. Therefore, the verification of the 3D model has been done successfully.

3 Research Methodology

Time history analysis (THA) is a dynamic structural analysis method that utilizes earthquake records to derive structural dynamic responses. Response spectrum analysis (RSA) method is often encouraged to be used by most earthquake codes due to its simplicity and time efficiency while the THA remains a more reliable technique to evaluate structural dynamic behavior. That is why, in this study, the THA method is employed for structural analysis.

Throughout the THA analyses, it is assumed that all structural members remain within the elastic range. All nonlinear behaviors, including structural or geometric nonlinearities, are not considered during the analyses. The finite element model of the structure is made utilizing the SAP2000 structural software [29]. Consequently, the THA analyses of the structure are performed, and the results for each loading situation are recorded for evaluation purposes. MATLAB [30] is also employed to plot graphs and figures by using the
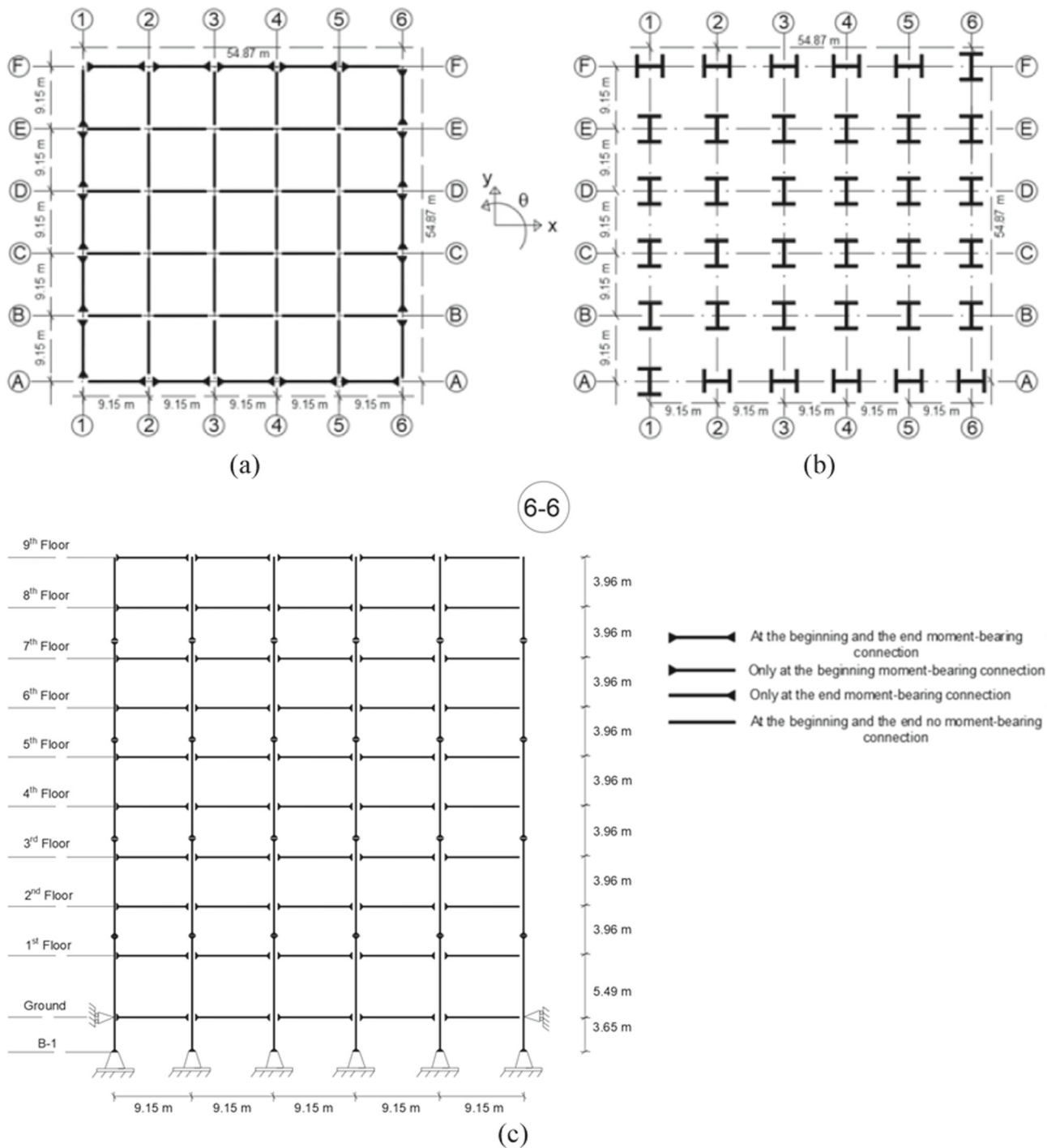
Fig. 2 Details of the 9-story Benchmark building; **a** beam-column connections **b** column layout view in plan and **c** elevation view of 6–6 axis

	Mode no	Dominant dir	3D Benchmark Building	Ohtori et al. [28]	Difference (%)
Table 2 The first nine frequency modes of 3D Benchmark building modeled by SAP2000 (Unit: Hz)	1	x-	0.415	0.443	6.7
	2	y-	0.417	–	–
	3	Q-	0.587	–	–
	4	x-	1.178	1.180	0.1

Table 2 (continued)

Mode no	Dominant dir	3D Benchmark Building	Ohtori et al. [28]	Difference (%)
5	y-	1.215	–	–
6	Q-	1.621	–	–
7	x-	2.049	2.050	0.1
8	y-	2.149	–	–
9	Q-	2.799	–	–

Fig. 3 A flowchart for research methodology
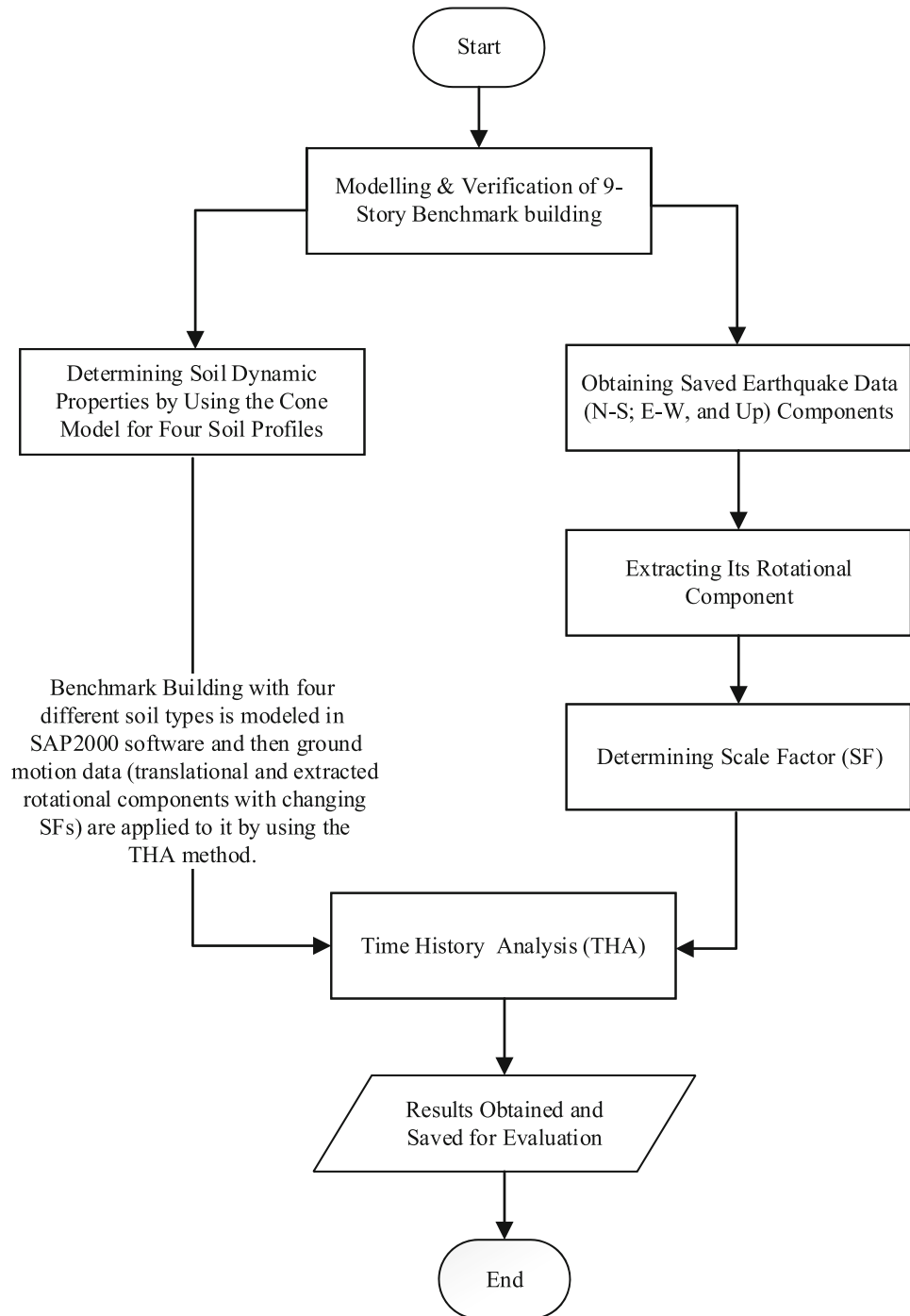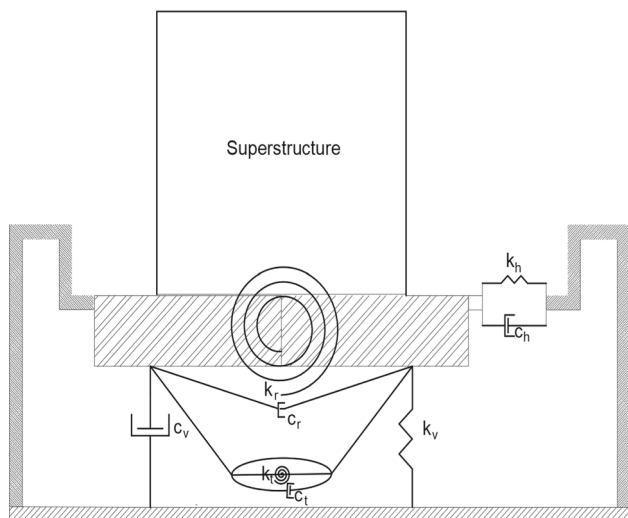
Fig. 4 Schematic view of the Cone model with equivalent dynamic parameters in the soil-half space considering SSI (horizontal, vertical, rocking, and torsional components)

obtained results in this study. A flowchart for the research methodology is also provided as shown in Fig. 3.

3.1 Soil–Structure Interaction (SSI)

Even if a building is constructed in compliance with all building codes and regulations, it can still be more susceptible to earthquake damage if the soil–structure interaction (SSI) effect is ignored [31, 32]. Recent seismic events have demonstrated that the dynamic behavior of buildings is influenced by the SSI, regardless of their quality of construction. Consequently, there has been growing interest amongst researchers [33–38] in the SSI as an important factor in developing more realistic system models for seismic analysis.

The present study employs mass-dashpot-spring models of the Cone model to simulate soil–structure interaction (SSI) effects. This approach is aimed at producing a more accurate representation of the dynamics involved in the Cone model [39]. While most researchers usually consider the earthquake's translational and rocking components in seismic analysis, this study includes the torsional components of the earthquake in the analysis as well. The Cone model, with all the equivalent dynamic parameters of the soil half-space, is shown in Fig. 4.

To model the effect of soil–structure interaction (SSI), the Cone model employs mass-dashpot-spring models in four different directions: horizontal, vertical, rocking, and torsional. For each direction, coefficients for stiffness (k), dashpot (c), and dimensional (γ) can be calculated using equations as seen in Table 3. The Winkler (mass-dashpot-spring) model of the SDOF system including the SSI effect is also illustrated in Fig. 5.

Where k_h, k_v, k_r, and k_t are, respectively, the equivalent stiffness elements representing soil characteristic dynamics in four different directions: horizontal, vertical, rocking, and torsional. Similarly, the variables (c_h, c_v, c_r, and c_t) for these directions can be calculated by using the same equation with different dimensional coefficients. Other variables in Table 3 include G, which is the shear modulus, V_s, the shear wave velocity, V_p, the dilatational-wave velocity, ρ, the density, and υ, the Poisson ratio of the site soil and M, the mass moment of inertia of the entire structure, where m, I, and k represent the mass, moment of inertia, and stiffness of the single-degree-of-freedom system (SDOF), respectively, and m_0 and I_0 are the mass and moment of inertia of the foundation system. The displacements (u_h, u_r and u_t) represent, in order, the lateral structural responses due to the horizontal, rocking, and torsional components of the ground motion while u_s is the lateral response of the structure. The angles ($\emptyset$ and θ) are symbolled as the rocking and torsional angles.

To calculate V_s and V_p, it is recommended to use Eqs. (1), (2) in order. If the Poisson ratio is $\upsilon \leq 1/3$, then it is recommended to calculate damping using V_p. However, if it lies between $1/3 < \upsilon \leq 1/2$, it is suggested to use $2V_s$ to compute the damping properties for the vertical and rocking components. For all values of the Poisson ratio, damping calculations should be made using V_s for the horizontal and torsional components. The types of soil sites used in the THA analysis are also listed in Table 4.

$$V_s = \sqrt{\frac{G}{\rho}} \tag{1}$$

$$V_p = \sqrt{2\frac{G}{\rho}\left(\frac{1-\upsilon}{1-2\upsilon}\right)} \tag{2}$$

Assuming that all columns at level B-1 are placed on a single footing that measures 4 m in two orthogonal directions, the dynamic properties of the Cone mode are calculated based on this footing size. The variables r_{0h}, r_{0v}, r_{0r}, and r_{0t} represent the equivalent radius of the foundation in the relevant directions, namely horizontal, vertical, rocking, and torsional. These variables are computed using the following Eqs. (3)-(5), respectively:

$$r_{0h}, r_{0v} = \sqrt{\frac{A_0}{\pi}} \tag{3}$$

$$r_{0r} = \sqrt[4]{\frac{4I_0}{\pi}} \tag{4}$$

$$r_{0t} = \sqrt[4]{\frac{2I_0}{\pi}} \tag{5}$$

where A_0 and I_0 are also the cross-sectional area and the second moment of area of the footing, respectively. The stiffness

Table 3 Equations to obtain soil dynamic properties by using the Cone model [39]

Types of earthquake components	Stiffness coefficient (k)	Dashpot (damping) coefficient (c)	Dimensionless damping coefficients (γ)
Horizontal	$k_h = \frac{8Gr_{0h}}{2-v}$	$c_h; c_t = \frac{r_{0h};r_{0t}}{V_s}\gamma k$	0.58
Vertical	$k_v = \frac{4Gr_{0v}}{1-v}$	or $c_v; c_r = \frac{r_{0v};r_{0r}}{Vp \text{ or } 2Vs}\gamma k$	0.85
Rocking	$k_r = \frac{8Gr_{0r}^3}{3(1-v)}$		$\frac{0.3}{1+\frac{3(1-v)M}{8r_{0r}5\rho}}$
Torsional	$k_t = \frac{16Gr_{0t}^3}{3}$		$\frac{0.433}{1+\frac{2M}{r_{0t}5\rho}}\sqrt{\frac{M}{r_{0t}5\rho}}$
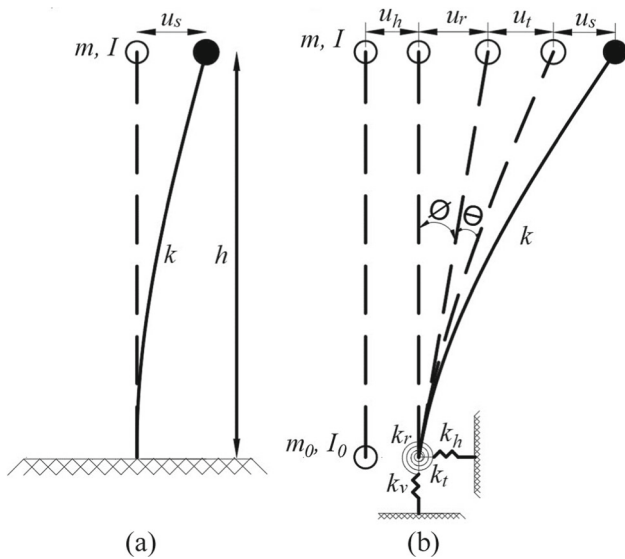
Fig. 5 Single-degree-of-freedom (SDOF) system: **a** fixed-base system, **b** soil structure interaction system

Table 4 Properties of soil site type

Soil type	G (kN/m^2)	V_s (m/sn)	ρ (ton/m^3)	v
Very soft	4000	50	1.60	0.49
Soft	18,000	100	1.80	0.49
Medium	171,000	300	1.90	0.48
Dense	600,000	500	2.40	0.33

notable because it was the first recorded earthquake in close proximity to an active fault line. For this reason, in this study, the data of the earthquake that occurred in El Centro on May 18, 1940 was used see Fig. 6 and these data were obtained from the 'PEER Ground Motion Database—PEER Center' [40].

and damping properties of site soil are calculated using equations and design criteria proposed by Wolf [39]. The results are tabulated in Table 5.

3.2 Ground Motion

Throughout history, there have been many devastating earthquakes. One that earthquake engineers are particularly familiar with is the El Centro earthquake. This earthquake is

3.3 Extracting a Rotational Component from Recorded Translational Earthquake Data

An earthquake releases a large amount of energy, mostly as seismic waves. An isolated point on the ground surface is represented by an elastic half-space, which is the site of the measuring system. An earthquake has three translational (displacements $u(t) = [u_x(t)\ u_y(t)\ u_z(t)]^T$) and three rotational components around Cartesian coordinates (angular displacement $\omega(t) = [\omega_x(t)\ \omega_y(t)\ \omega_z(t)]^T$) as shown in Fig. 7. Here, the fundamental characteristics of linear elas-

Table 5 The calculated stiffness and damping properties of site soil in the relevant direction

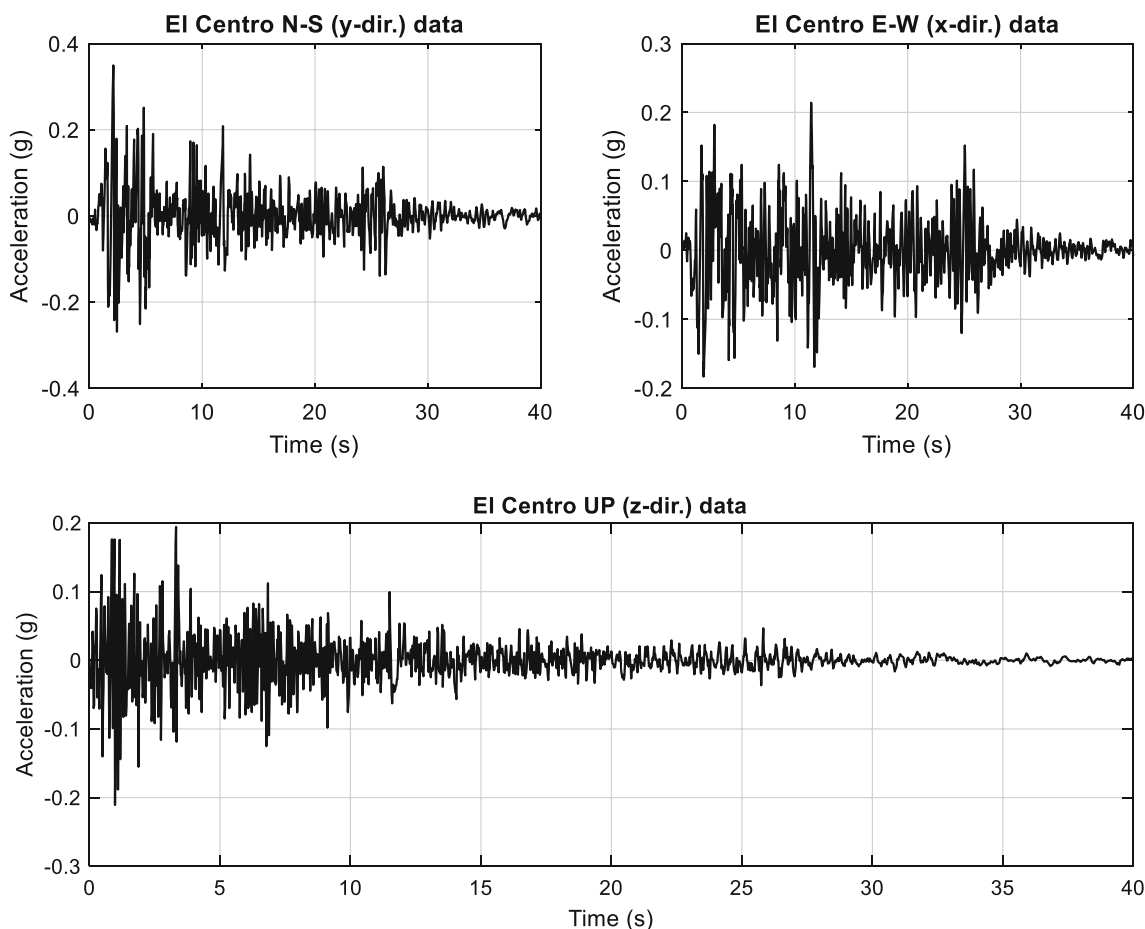| Soil	k_h (kN/m)	k_v (kN/m)	k_r (kN/m)	k_t (kN/m)	c_h (kNs/m)	c_v (kNs/m)	c_r (kNs/m)	c_t (kNs/m)
Very soft	47,825	70,800	10,997	6670	1251	1358	0.97	1.08
Soft	215,214	318,601	49,489	30,015	2816	3055	2.44	2.57
Medium	2,031,082	2,968,505	461,108	285,143	8861	9490	7.82	8.36
Dense	6,486,491	8,083,910	1,255,702	1,000,504	16,980	15,622	12.64	19.78

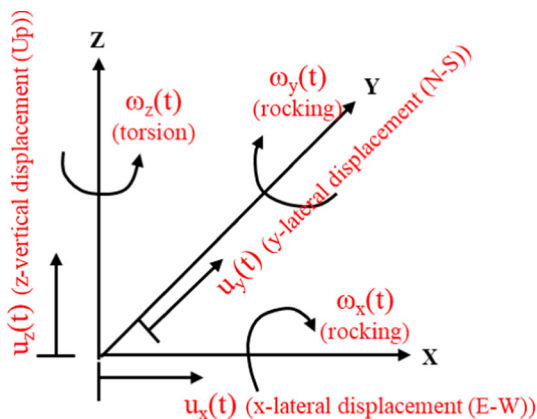**Fig. 6** N-S; E-W; and UP data of the 1940 El Centro earthquake

Fig. 7 Representation of six components of an earthquake

ticity are employed relevant to understanding the rotational motions associated with seismic waves [10].

Let us define seismic transverse wave functions in three orthogonal directions as given in Eqs. (6)-(8) where, A_x, A_y, and A_z are, respectively, the amplitude of the seismic waves; and k_x, k_y, and k_z are the angular wave numbers; and ω_x, ω_y,

and ω_z are the angular frequencies in the relevant directions.

$$u_x(t) \rightarrow u_x(y, t) = A_y \cos(k_x y - \omega_x t) \tag{6}$$

$$u_y(t) \rightarrow u_y(x, t) = A_x \cos(k_y x - \omega_y t) \tag{7}$$

$$u_z(t) \rightarrow u_z(x, y, t) = A_z \cos(k_z y - \omega_z t) + A_z \cos(k_z x - \omega_z t) \tag{8}$$

The body dynamic equations by using the linear elastic method correspond to the antisymmetric part of the spatial gradient tensor of the displacement field $u(t)$ (m) to rigid body rotation $\omega(t)$ (rad), as follows:

$$\begin{Bmatrix} \omega_x(t) \\ \omega_y(t) \\ \omega_z(t) \end{Bmatrix} = \frac{1}{2} \nabla x u(t) = \frac{1}{2} \begin{pmatrix} \frac{\partial u_z(t)}{\partial y} - \frac{\partial u_y(t)}{\partial z} \\ \frac{\partial u_x(t)}{\partial z} - \frac{\partial u_z(t)}{\partial x} \\ \frac{\partial u_y(t)}{\partial x} - \frac{\partial u_x(t)}{\partial y} \end{pmatrix} \tag{9}$$

In here, ∇x is the nabla (curl) operator. At the free surface, assuming stress-free boundary conditions and noting that our

observables are rotational velocities (rad/s), one obtains:

$$\begin{Bmatrix} \dot{\omega}_x(t) \\ \dot{\omega}_y(t) \\ \dot{\omega}_z(t) \end{Bmatrix} = \frac{1}{2}\nabla x \dot{u}(t) = \begin{pmatrix} \frac{\partial \dot{u}_z(t)}{\partial y} \\ -\frac{\partial \dot{u}_z(t)}{\partial x} \\ \frac{1}{2}\left(\frac{\partial \dot{u}_y(t)}{\partial x} - \frac{\partial \dot{u}_x(t)}{\partial y}\right) \end{pmatrix} \quad (10)$$

After substitution and rearranging Eq. (10), then the equation becomes as:

$$\begin{Bmatrix} \dot{\omega}_x(t) \\ \dot{\omega}_y(t) \\ \dot{\omega}_z(t) \end{Bmatrix} = \frac{1}{2}\nabla x \dot{u}(t) = \begin{pmatrix} \frac{1}{c}(\ddot{u}_z(t)) \pm \varphi_{\text{add}} \\ -\frac{1}{c}(\ddot{u}_z(t)) \pm \mu_{\text{add}} \\ \frac{1}{2c}(\ddot{u}_x(t) - \ddot{u}_y(t)) \end{pmatrix} \quad (11)$$

Here, c is the shear-phase velocity, which is considered to be 3600 m/s^2; φ_{add} and μ_{add} are the additional rocking components due to other seismic wave contributions (reflected SV wave, Love wave, etc.) and some uncertainties (noise, etc.) in the relevant directions. For this study, only the torsional component is computed and used for all rotational components in dynamic analyses.

Extracted rotational (torsion one) component of 1940 El Centro and its Fourier transform for use as a rotational component in the THA analyses are given in Fig. 8. For more details about extracting the rotational motion from the saved earthquake data, readers refer to studies [7–11].

3.4 Scale Factors (SFs)

Earthquakes are unpredictable natural events that are characterized by numerous uncertainties. While mathematical modeling allows us to extract rotational components, there are still uncertainties that must be addressed. Moreover, each earthquake can have a different frequency/amplitude context and direction. To address these challenges, scale factors (SFs) are proposed by incorporating the building radius of gyration and the rate of saved translational one to obtain rotational components. By doing so, it becomes possible to take into account different amplitudes that may occur during an earthquake.

The study objective is to investigate the influence of earthquake rotational components on structural dynamic responses. To achieve this, the scale factor (SF) of the rotational component of the earthquake is enlarged with either a negative or positive coefficient based on the earthquake's directivity effect and applied to the model (Benchmark) buildings with the help of the SAP2000 software. The data of the rotational components, as shown in Fig. 8, remain the same and are used for all rocking and torsional components, except for different scale factors. The scale factors (SF$_x$, SF$_y$, and SF$_z$) were determined using Eqs. (12) - (14) with the rotation scale factors around the x-, y-, and z-directions, respectively. The scale factors are limited within a certain

range, assuming that the rotational data of the earthquake is equal to or less than the vertical data in the maximum relevant direction. The limitations are also given below in the following order for each direction.

$$0 \leq \text{SF}_x \leq \frac{\max|T_z|}{\max|Q_x| \cdot r_y} \quad (12)$$

$$0 \leq \text{SF}_y \leq \frac{\max|T_z|}{\max|Q_y| \cdot r_x} \quad (13)$$

$$0 \leq \text{SF}_z \leq \frac{\sqrt{\left(\frac{\max|T_x|}{r_y}\right)^2 + \left(\frac{\max|T_y|}{r_x}\right)^2}}{\max|Q_z|} \quad (14)$$

$$r_x = \frac{L_x}{\sqrt{12}}, \ r_y = \frac{L_y}{\sqrt{12}}, \ r = \sqrt{r_x^2 + r_y^2} \quad (15)$$

Here, max $|Q_x|$, max $|Q_y|$, and max $|Q_z|$ represent the maximum absolute value in the rotational data in the x-, y-, and z-directions of the earthquake, they are the same because the same rotational data as seen in Fig. 8 are used for rocking and torsional component. max$|T_x|$, max$|T_y|$ and max$|T_z|$ represent the maximum absolute value of the translational components (records) of the earthquake in the x-, y-, and z-directions, see Fig. 6. As for the other notations, r_x and r_y represent the radius of rotation in the x- and y-directions, while r is the total radius of rotation of the building. In addition, L_x and L_y show the total length of the building in the x- and y-directions.

The Benchmark building has a symmetric plan and load-bearing members without leading to geometric eccentricity for both x- and y-directions. It is expected to give the same response for those directions. Therefore, SF$_r$ is only employed instead of using two different scale factor coefficients (SF$_x$, SF$_y$). In addition to that, SF$_z$ represents the torsional scale factor, and it can be renamed as SF$_t$.

4 Results and Discussion

An earthquake consists of surface and body waves such as S-, P-, Love, and Rayleigh waves. Each one of them has special characteristic effects when spreading through different soil types. Due to the incident and reflection of those waves, earthquakes can have rotational (rocking and torsional) components besides translational ones. Most of the current earthquake codes can neglect the rotational components except for some special structure constructions in the dynamic analyses. However, in this study, to examine the earthquake rotational components on structural dynamic responses, the rotational component of the earthquake is extracted from its recorded earthquake component by using the linear elastic method, and its effect is extended by using

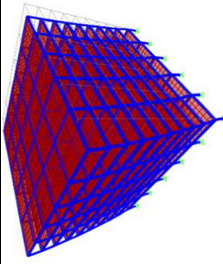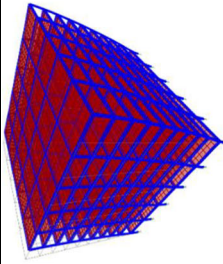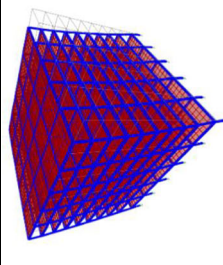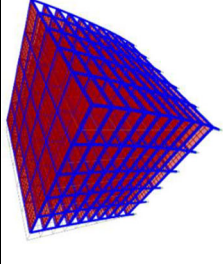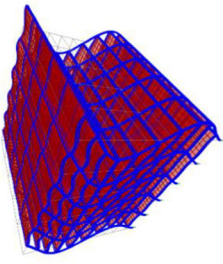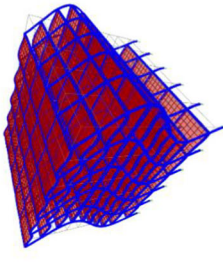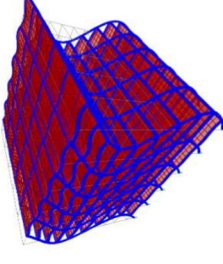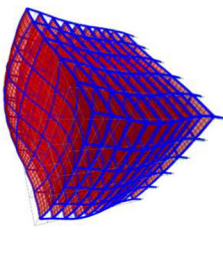**Fig. 8** 1940 El Centro earthquake rotational component and its Fourier transform
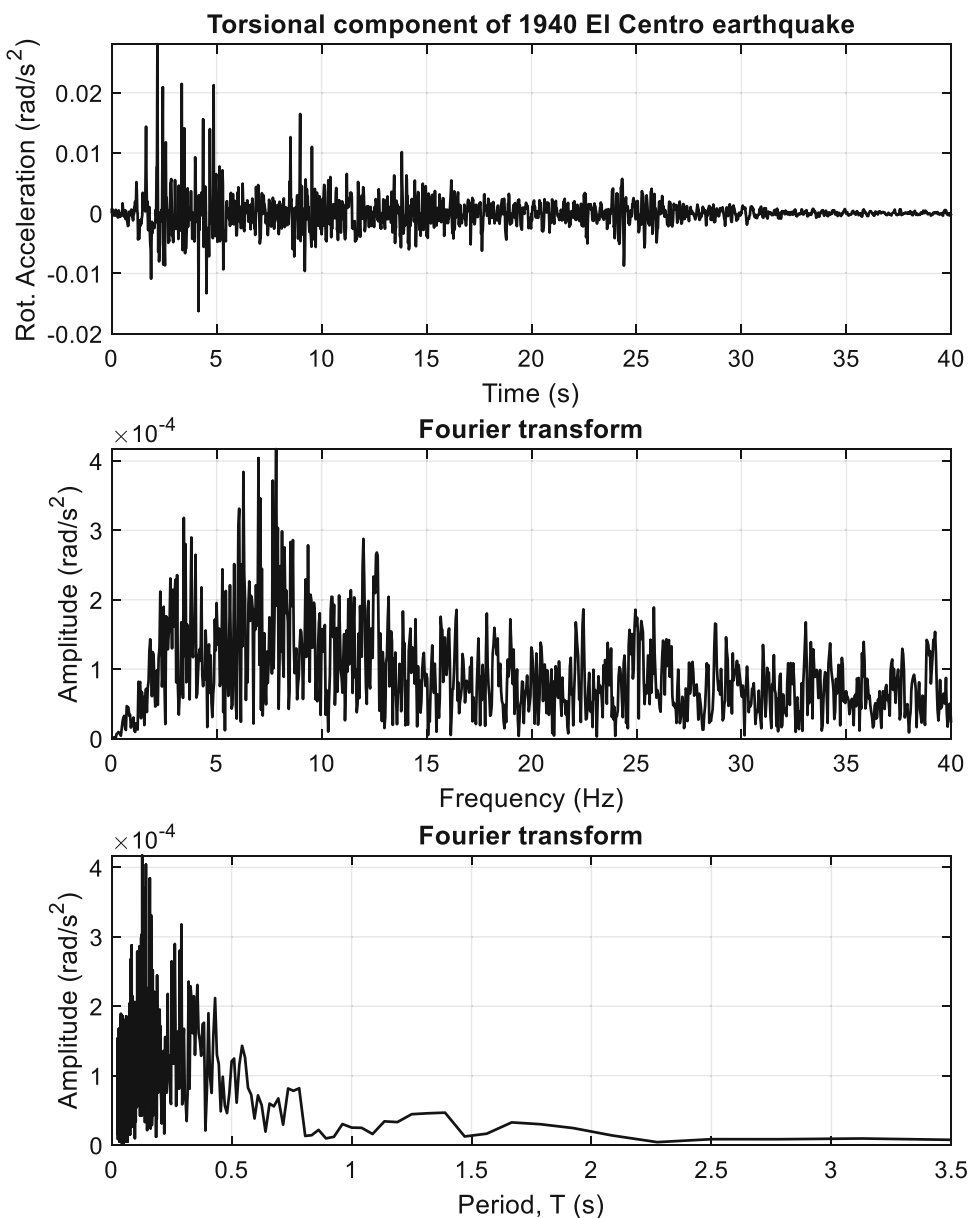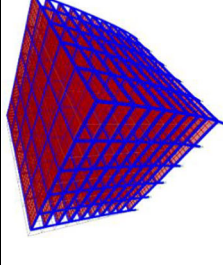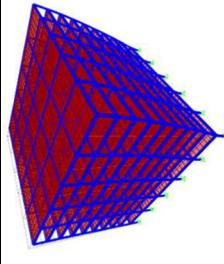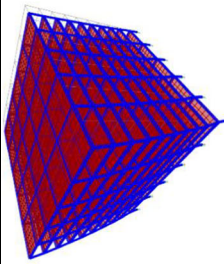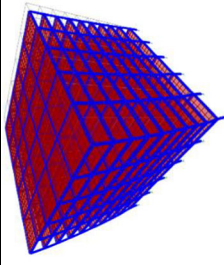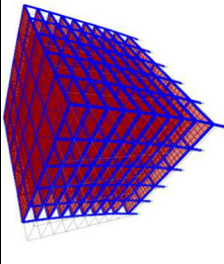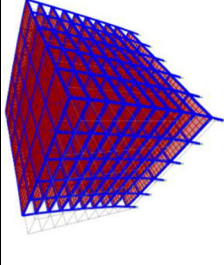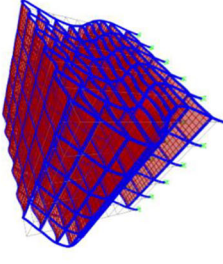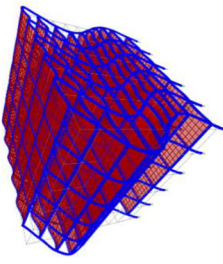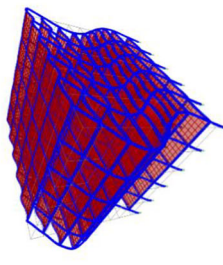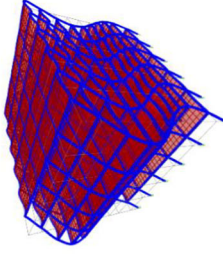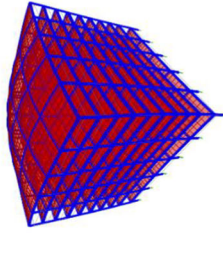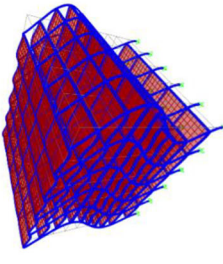
the scale factor that was defined previously in Sect. 3.3. For the directivity effect of the earthquakes, the SFs can take positive and negative values.

THA analyses are conducted in the case of the Benchmark building placed on very soft, soft, medium, and dense soil types. Thanks to that, the soil structure interaction (SSI) effect is planned to be performed once the dynamic analyses are made. Thus, the evaluation criteria are determined as the period, base shear, inter-story drift ratio, maximum floor acceleration, and earthquake input energy to examine how the rotational ground motion affects the dynamic responses of the structure including the SSI effects.

4.1 Modal Analysis (MA)

The analysis of modal properties plays a crucial role in extracting and characterizing the dynamic characteristics of a structure [41, 42]. In this study, an analysis of fixed-based and Benchmark buildings with different soil types was conducted to examine the influence of soil–structure interaction (SSI) on structural dynamic responses for the first fifteen modes. Critical modes and modal shape illustrations for the Benchmark building with different soil profiles are determined and presented in Fig. 9. For detailed information regarding the modal analyses, please refer to the tables in Appendix 1.

Fig. 9 Selection of critical modes and modal shape illustrations for Benchmark building with different soil profiles

As illustrated in Fig. 9, the first mode (M.1) of the Benchmark building under a fixed-based condition exhibits a predominantly lateral mode in the x-direction, with a modal mass participation ratio ($U_x = 0.792$). Meanwhile, the Benchmark building with varying soil types, including soil–structure interaction (SSI) effects, demonstrates dominant lateral modes in the *y*-direction. Similar observations are noted for the second mode (M.2). However, in the case of the seventh mode (M.7), the Benchmark building situated on very soft soil displays a dominant mode in the gravitational direction, with a mass participation ratio value of ($U_z = 0.89$). Conversely, the other conditions exhibit coupled (lateral-rocking) modes.

Furthermore, it is noteworthy that the Benchmark building on very soft soil displays a dominant rocking mode around the *y*-direction ($R_y = 0.464$) for the eighth mode (M.8), while the rest of the conditions exhibit coupled (lateral-rocking) modes. In conclusion, as soil properties deteriorate (from dense to very soft soil type), structural models are likely to encounter unpredictable challenges and damages when employing the fixed-based method in seismic analysis. This is due to the increasing dominance of gravitational and rotational, especially rocking modes in the total response. If these modes are excited by one or more earthquake components individually or simultaneously, their effects become even more crucial. Consequently, this stresses the importance of integrating SSI effects exposed to earthquake rotational components into dynamic analyses.

Table 6 presents the first three periods of the Benchmark buildings, considering soil–structure interaction across various soil types. Upon the assessment, the fundamental periods of the structures are determined to be 2.63 s, 2.67 s, 2.92 s, and 3.2 s for dense, medium, soft, and very soft soils, respectively. The analysis of the soil type effects on the structural response reveals a consistent increase in building periods from dense soil to very soft soil. For instance, the first period of the building with very soft soil is 21% and 33% higher than that on dense soil and fixed base in order.

The modal mass participation ratio (MPR) demonstrates an increasing trend concurrent with the deteriorating soil conditions. For instance, in the case of very soft soil type, the MPR in the torsional direction is ($R_z = 0.90$), whereas it is 0.83 for the fixed base condition. Furthermore, the MPR values for the dominant lateral modes like the first and second modes, have also shown an increase from $U_x = 0.79$ and $U_y = 0.79$ to $U_x = 0.88$ and $U_y = 0.88$. This phenomenon may be attributed to the amplification of soil–structure interaction (SSI) effects, resulting in an increased building height and consequently, an extended building period. However, it is important to note that this consequence is not solely due to the aforementioned factor, but also due to the emergence of rotational modes as dominant even in the lateral direction. This exhibits the significant influence of soil–structure interaction

on critical dynamic characteristic parameters, particularly the periods of the structure.

4.2 Base Shear (BS)

Base shear (BS) is a dynamic indicator to test overall structural performance in dynamic analyses. Therefore, in this study, analyses are carried out to determine the maximum base shear forces based on soil types, accounting for rocking and torsional components. Figure 10 presents a change in the BS by applying rocking and torsional earthquake components with varying SF_r and SF_t. The red dot in the center of Fig. 10a–d indicates the base shear force when the earthquake's rocking and torsional scale factor (SF_r and SF_t) coefficients are zero meaning that the rotational components of the earthquake are not considered. They are bounded between -10 and 10 to take critical earthquake direction into account and negative ($-$) and positive ($+$) sign shows the earthquake direction.

Figure 10 shows the base shear forces change according to soil types: dense, medium, soft, and very soft, respectively, in consideration of whether or not the earthquake's rotational components are considered. Without the rotational component of the earthquake, the maximum base shear forces on dense, medium, soft, and very soft soil, respectively, occur at 30,864.03, 29,375.66, 26,318.95, and 23,215.51 kN. However, when the rocking and torsional components are taken into account, the corresponding base shear forces are 34,773, 33,348, 27,090, and 23,589 kN for the relevant soil types in order. Furthermore, the percentage differences take place between 1.6 and 13% increase from very soft through dense soil type once considering the rotational components. It means that the rotational component of the earthquake can affect the base shear of whatever type of soil the structure is located on, but the maximum change occurs in the stiffer soil types such as dense and medium soils.

Moreover, when the SF_t gets values between -10 and 10, the change in the base shear remains almost stable while the base shear change is significantly affected by the SF_r getting values within the same boundary. This shows that the torsional component of the earthquake does not affect the base shear force; however, the rocking component is found to be more effective for any soil-type condition under the Benchmark structure. It is also interesting to note that if the SF_r increases in the ($-$) direction, the base shear force increases especially for dense and medium soil types, and vice versa. This situation in this study is called the directivity effect (DE) of the rotational component of the earthquake. This shows that the rocking component SF_r coefficient and its direction of the earthquake are more critical to the base shear forces in buildings.

Table 6 The first three periods of the benchmark building with different soil types (unit: s)

Period	Very soft soil			Soft soil			Medium			Dense			Fixed base		
	P	M.P.R	D.D	P	M.P.R	D.D	P	M.P.R	D.D	P	M.P.R	D.D	P	M.P.R	D.D
1	3.21	0.88	U_y	2.92	0.87	U_y	2.68	0.84	U_y	2.63	0.83	U_y	2.41	0.79	U_x
2	3.18	0.88	U_x	2.88	0.87	U_x	2.67	0.84	U_x	2.63	0.83	U_x	2.40	0.79	U_y
3	2.16	0.90	R_z	2.03	0.88	R_z	1.89	0.84	R_z	1.86	0.83	R_z	1.70	0.83	R_z

P period; *M.P.R* modal participation ratio; *D.D* dominant direction
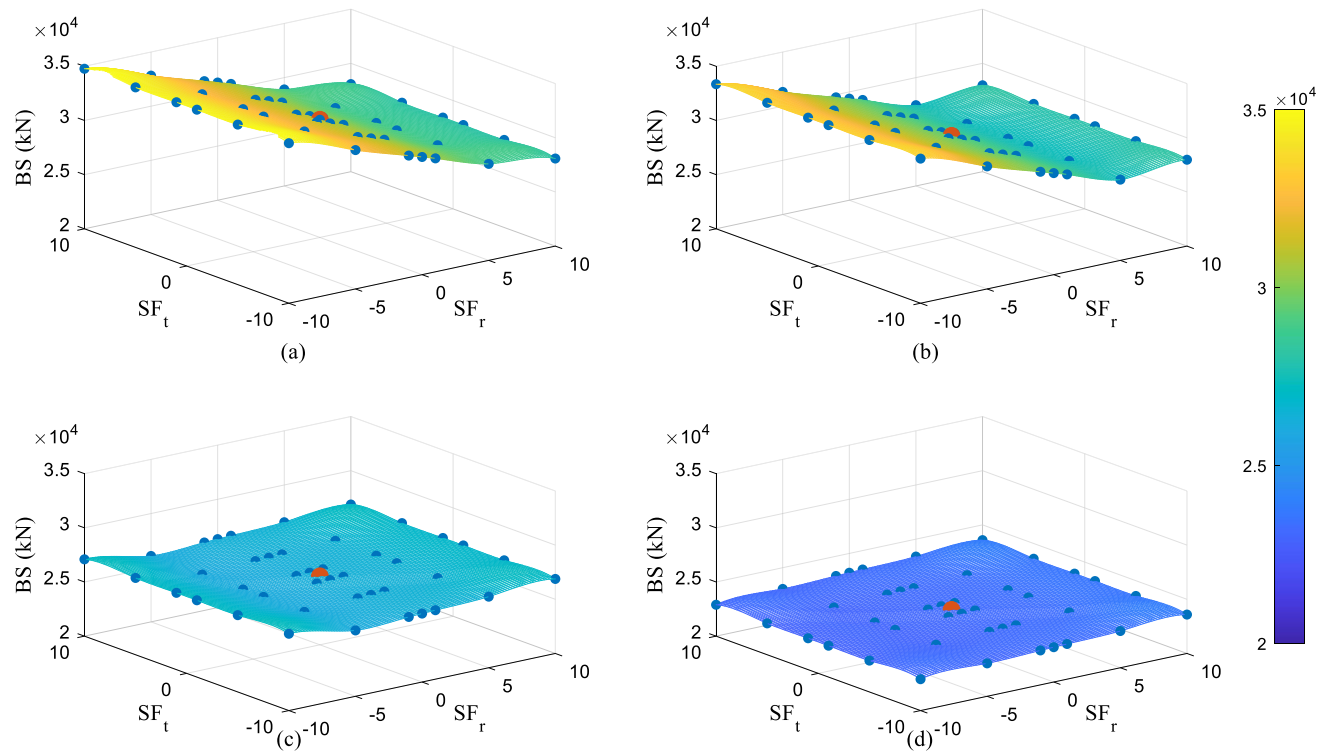
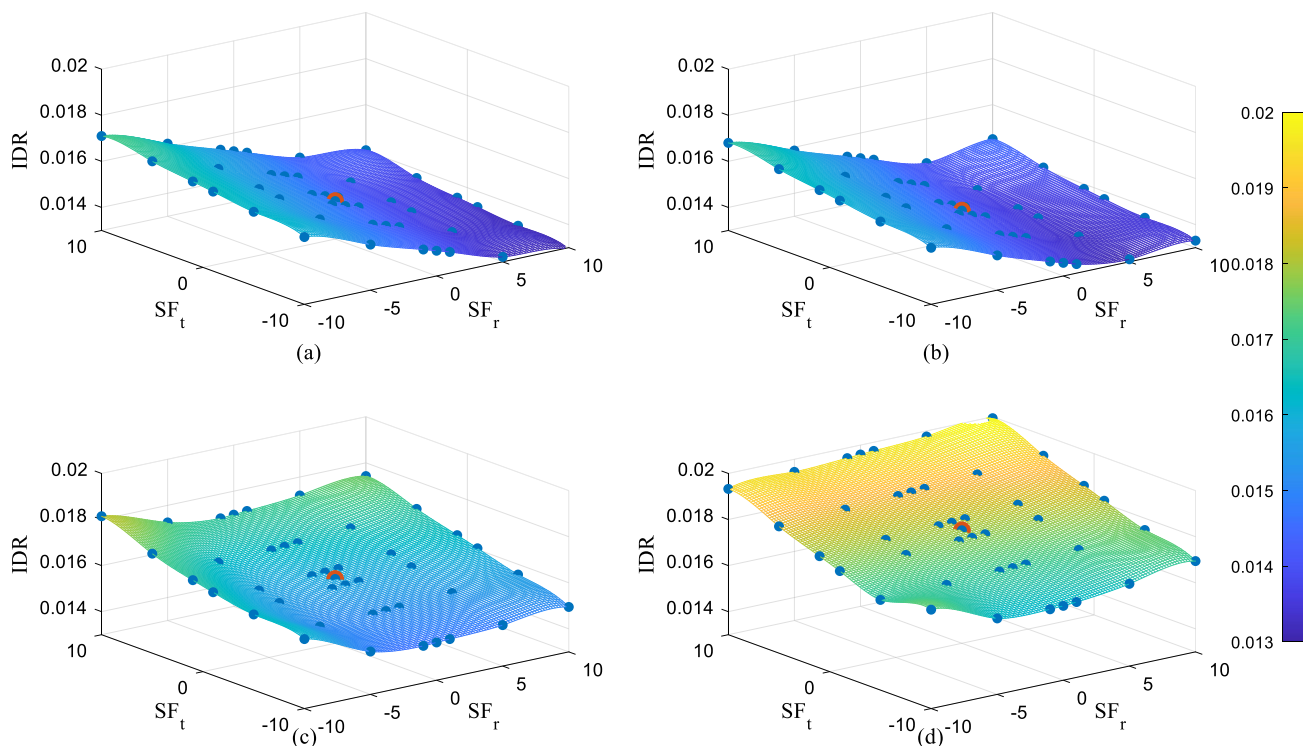

Fig. 10 Base shear forces according to soil types: **a** dense, **b** medium, **c** soft, **d** very soft

4.3 Inter-Story Drift Ratios (IDRs)

Another useful criterion to test the structural performance is the inter-story drift ratio (IDR). As a result of the THA analyses, the maximum IDRs obtained according to soil types, depending on the rocking and torsional components, are shown in Fig. 11.

As looking at Fig. 11, as rocking and torsional components are not considered in the analyses, the maximum IDRs in dense, medium, soft, and very soft soils are 0.0146, 0.0142, 0.0157, and 0.0179, respectively. When they are taken into account, the values are obtained as 0.01709, 0.0168, 0.0181, and 0.0199, in order. Considering these values, the inclusion of the rocking and torsional ground motion components increases the IDRs in the building by up to 16.72%, 18.02%, 14.88%, and 11.35%, respectively, in dense, medium, soft, and very soft soils.

When it comes to evaluating the effect of soil types on the IDR index, there is an overall increase of IDRs for any type of soil because the IDRs vary depending on the soil type. It is figured out that both the rocking and torsional components of the ground motion affect the IDRs in the building. While the effect of the torsional earthquake component on the IDR index becomes more dominant as compared to the rotational one for soft and very soft soils, the rocking component becomes more effective in dense and medium soils. If only the torsional component is taken into account, the increases as compared to the building exposed to only translational components of the earthquake are limited to approximately 4.7% in dense and medium soils; however, increases of up to about 9.4% are observed on soft and very soft grounds. Unlike the base shear, the torsional component is becoming more effective and should not be ignored in the IDRs index.

Fig. 11 The maximum inter-story drift ratios (IDRs) according to soil types: **a** dense, **b** medium, **c** soft, **d** very soft

In addition to that, the directivity effect of the rotational ground motions is observed like the base shear index. It means that if the SF_r gets values increasingly from zero to ten in the (+) direction, the IDR index slightly increases for soft and very soft soil and vice versa; however, it does not work for dense soil and medium soil types. That shows how important the directivity effect is under consideration of the rotational components in the dynamic analyses.
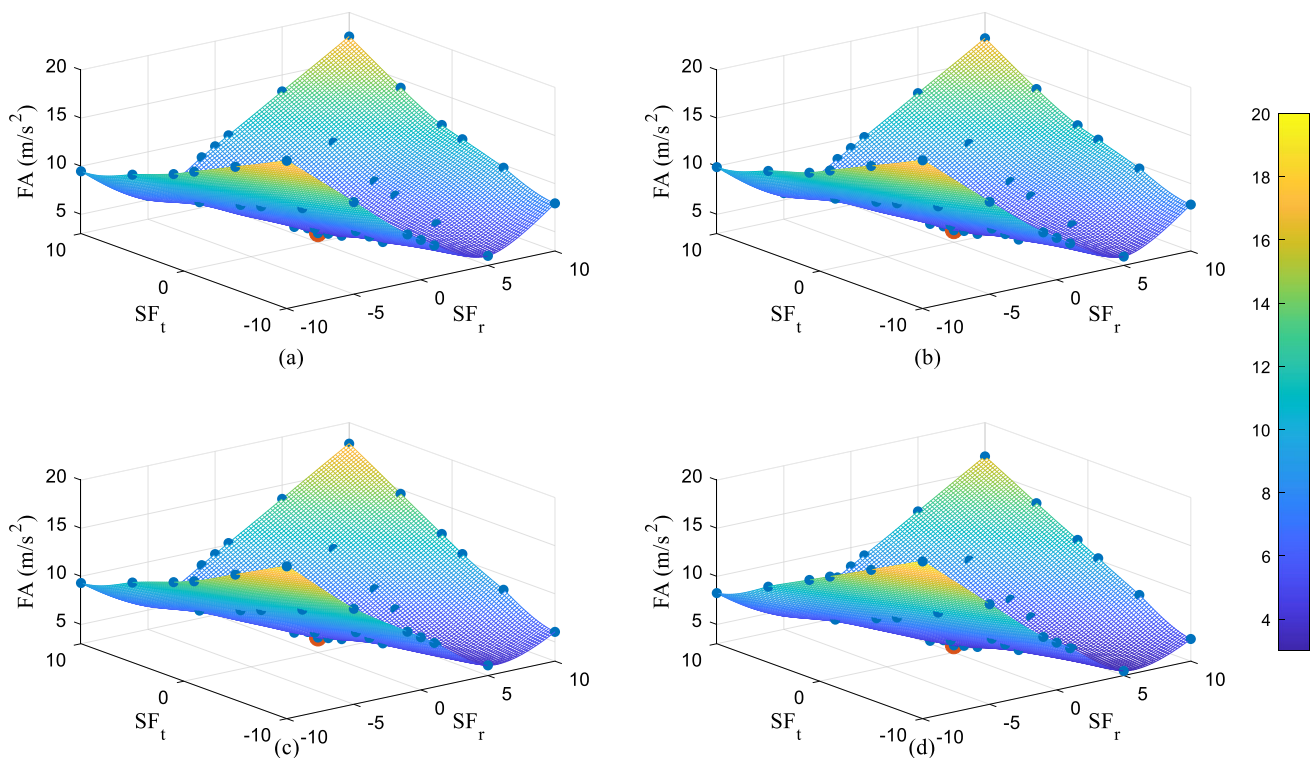
4.4 Floor Accelerations (FAs)

The maximum FAs obtained according to soil types whether or not the rocking and torsional components are included in the THA analyses are shown in Fig. 12. If the rocking and torsional components are not considered in the analyses, the max. FAs are, respectively, 3.94, 4.25, 4.54, and 3.73 m/s^2 for dense, medium, soft, and very soft soils. In addition, the max. FAs are 4.22, 4.42, 4.85, and 3.98 m/s^2, respectively, as the rotational components are considered and its scale factors (SF_r and SF_t) equal to 1 while scale factors (SF_r and SF_t) are equal to 10, the max. FAs can get values as 18.34, 18.39, 18.82 and 19.33 m/s^2, respectively. When the effects of soil types on the max. FAs in the building are evaluated; it has been observed that both rocking and torsional components affect the max. FAs in the building than other structural response parameters, such as the BS and the IDRs.

4.5 Spectral Accelerations (SAs)

The graph in Fig. 13 shows the spectral accelerations (SAs) for the top floor of the building, with varying scale factors (SF_r and SF_t) taken into account for different types of ground. When both SF_r and SF_t are zero, it means that there are no rotational components of the earthquake considered in the dynamic analyses. Under this circumstance, the building situated on very soft soil has the lowest spectral acceleration, while the building on dense soil has the highest acceleration on the roof floor. When the scale factors are equal to one, there is a slight difference from the results without rotational components. However, when the scale factors are higher, such as five and ten, the rotational components of the earthquake dominate the structural response within 0–5 s of the period. After one second, the SAs for any type of soil with varying scale factors are either the same or show no significant change. This can be because the rotational earthquake components have limited effects after one second, as shown in Fig. 7 and Fig. 13.

In order to more clearly present the effects of the rotational components of the earthquake on the floor spectral accelerations, the spectral accelerations of the rocking and torsional components of the earthquake are obtained by using different scale factors as seen in Fig. 14. If the SF_r is zero, it means no rocking component is implemented and if the SF_t is zero, it means no torsional component is applied to the structure.

Fig. 12 The maximum floor acceleration obtained in the Benchmark building according to soil types: **a** dense, **b** medium, **c** soft, **d** very soft

Based on the analysis of the rocking and torsional components separately, it was found that the rocking component has a greater impact in the first half-second interval (0–0.5 s), while the torsional component has a greater impact in the second half-second interval (0.5–1 s). In general, the frequency contents of the rotational components of the earthquake have a considerable influence on the structural response parameters especially when the SF_s are getting higher. It is important to note that these findings on spectral accelerations are based on the historical earthquake record and model building used in the study. The behavior of structures and soil may vary in different building types and ground movements with different frequency contents.

4.6 Input Energy (IE)

The input energy (E_{ir}) is another important parameter to see the overall performance of the structure, which has a proportional relationship between structural relative velocity and ground excitation [43]. The total input energy of the Benchmark building located on the different soil types is obtained when the rocking (SF_r) and torsional (SF_t) coefficients are in the range of '− 10, + 10', which are illustrated in Fig. 13. If the (SF_r) and (SF_t) are zeros, it means that there are no rotational components considered in the analysis. The torsional components are taken into account for the rest when

the (SF_r) and (SF_t) are getting values in order as 1, 1; − 1, − 1; 5, 5; − 5, − 5; 10, 10; and − 10, − 10.

The max. seismic input energies obtained where both rocking and torsional components are considered increased by 8.34%, 7.89%, 14.42%, and 21.57%, respectively, in dense, medium, soft, and very soft soils, compared to the case when rotational components were not taken into account. When only the torsional component excluding rocking ones is considered, the change in the max. input energy as compared to that having only translation components can be up to 3% increase occurred for any type of soil. Considering this limited percentage increase, the effect of the torsional component of the earthquake on the seismic input energy becomes very limited, see Fig. 15.

For evaluating the seismic input energies according to soil types, the highest input energy happens in soft soil while the lowest input energy occurs in very soft soil. This can happen because the building does not have an adequate rigid connection between the foundation and the very soft soil so the earthquake input excitations cannot be transferred fully from the soil through the structure. Moreover, the foundation can move back and forward as if base isolations are implemented underneath it; therefore, the earthquake excitations are partially dissipated instead of fully transferring it. This effect is named as isolation effect (ISE) in this study.

Seismic input energy for varying scale factor coefficients in dense, medium, soft, and very soft soil is tabulated in
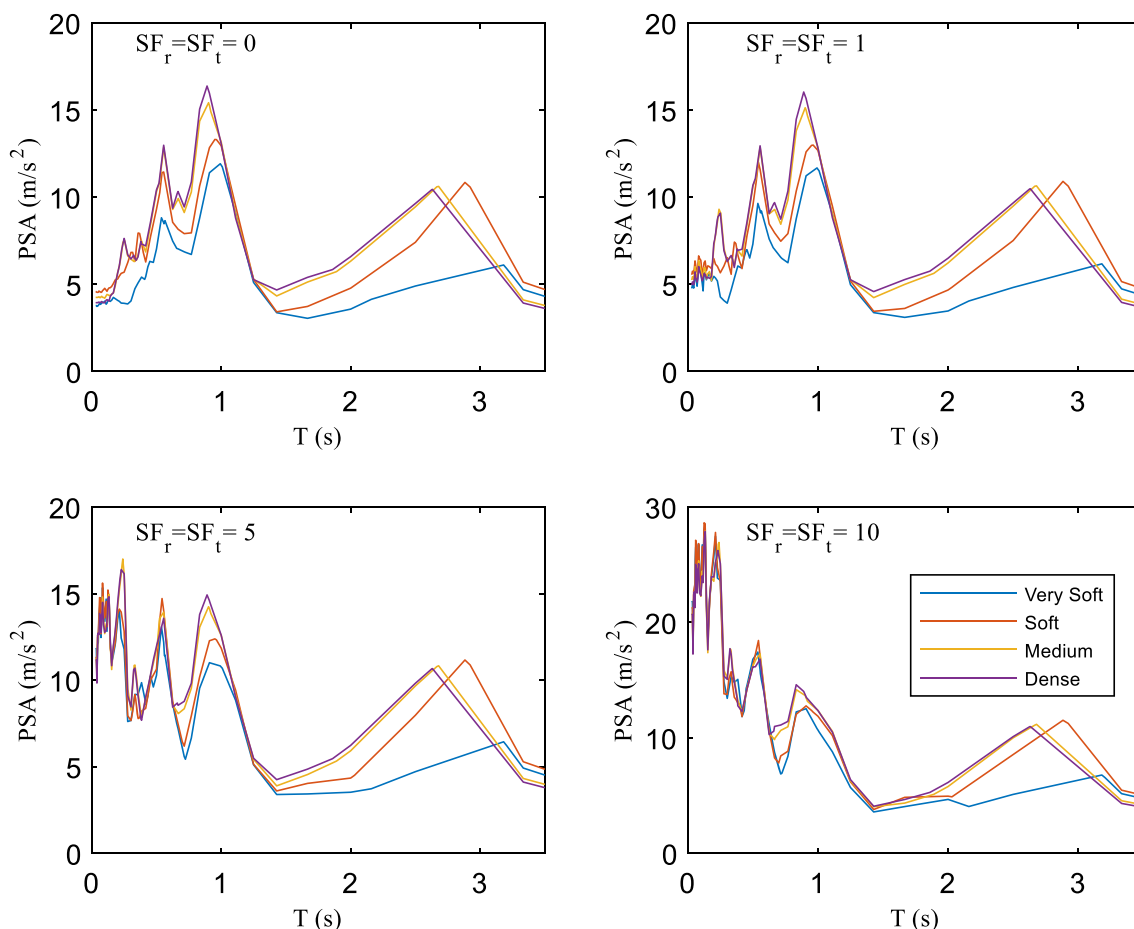
Fig. 13 Top (roof) floor spectral accelerations for different scale factors and soil types with % 5 damping

Table 7. In all soil types, when the SF_t increases in (−) and (+) directions, the input energy also increases, but it is still limited. In addition, while the SF_r increases in the (−) or (+) direction, the input energy has increased for any type of soil. Similarly, as the rocking scale factor (SF_r) coefficients increase in the (−) or (+) direction, the seismic input energies also increase. All in all, it is found that the rotational component scale factors and their directions have significant effects on the seismic input energies occurring in buildings.

5 Conclusion

The present study conducts linear analyses on the Benchmark 9-story steel structure, specially built for the SAC project in the USA. The analyses utilize the linear THA method, taking into account the earthquake's translational (vertical and horizontal) and rotational (rocking and torsional) components. Additionally, the analyses account for four different soil types with shear velocity 'V_s' values ranging from 50 to 500 m/s^2. The structure is modeled utilizing

the three-dimensional finite element method, with soil–structure interaction accounted for using spring-dashpot elements attached at the bottom foundation columns in the Benchmark building, utilizing the SAP2000 structural software. The analyses consider the effects of the rocking and torsional components of ground motion as well as the structure–soil interaction effects. It should be noted that the results presented in this study are for a 9-story building resting on four different soil types, and the study does not aim to provide a generalized analysis method covering all possible aspects of SSI modeling and rotational ground motion extraction. The effects of the earthquake rotational components on the structural performance indexes may vary for different building types. Based on the results, the following conclusions are drawn:

The modal analyses of the model building, accounting for soil–structure interaction (SSI) effects in comparison to a fixed-based model, demonstrate noteworthy changes not only in rotational modes (rocking and torsional) but also in lateral mode (z-direction: gravity direction). Furthermore, it results in an increased contribution of rotational modes to coupled or
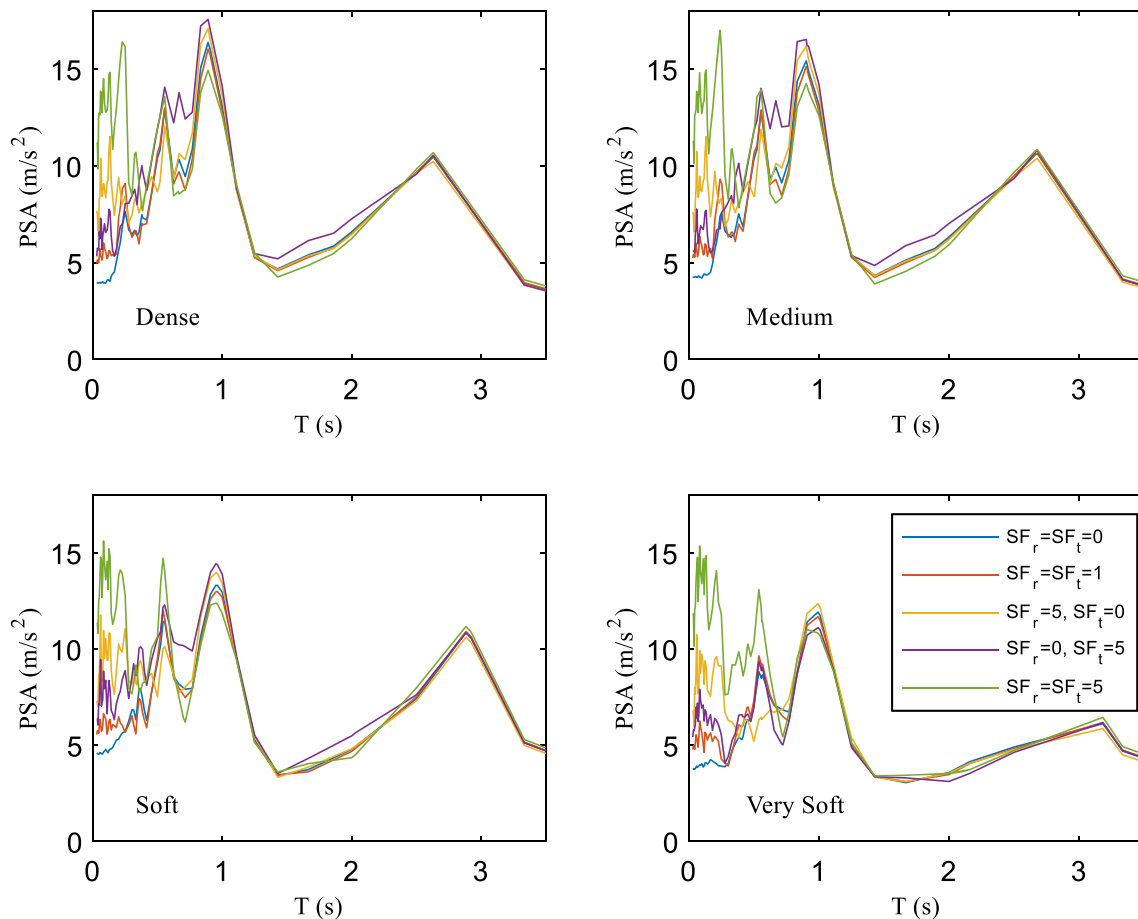
Fig. 14 Roof spectral accelerations for different scale factors and soil types with % 5 damping

dominant lateral modes, highlighting the significant impact of soil–structure interaction on critical dynamic characteristic parameters.

The fundamental period is a crucial dynamic parameter for structures, as it allows us to roughly and quickly measure how much earthquake energy a structure can withstand. According to that, the Benchmark structure placed in very soft soil exhibits a 21% percent increase in the first period of the structure compared to the one placed in dense soil. That shows how soil types play a significant role in the structural response characteristic. The rotational component of the ground motion can increase the base shear force in the building by 13.52%, maximum IDRs by 18.02%, and maximum seismic input energies by 21.57%. Although it varies depending on the soil type, it has been determined that both the rocking and torsional components affect the IDRs; however, the rocking component is more dominant in the building behavior.

Based on the results, it is evident that considering the rotational components of ground motion in dynamic analyses generally causes the BS and the IDR to be more affected as the ground shear velocity (V_s) increases. If only the torsional

component is considered, the IDR is conversely affected more as V_s decreases, except for the BS which is not affected by the torsional component of the soil. Furthermore, the effect of torsional and rocking components on the max. FAs and the IDRs show significant effects having similar trends for all soil types.

The directivity effect (DE) of the rotational component of the earthquake plays a significant role when considering the base shear and inter-story drift ratios whereas the DE effect has not been observed for the floor accelerations index. That means the rocking component SF_r coefficient and the direction of the earthquake become more critical.

When it comes to the SA index, it is seen that the rocking component dominates the response in the period interval (0–0.5 s), while the peak SA because of the torsional component takes place in the vicinity of the rocking one, which is the interval (0.5–1 s). Both components have impacted the structure with shorter periods. For this reason, the structure having a dominant mode or modes close to those intervals becomes more susceptible to earthquake rotational components. Furthermore, the frequency contents of the rotational components of the earthquake have a significant influence on
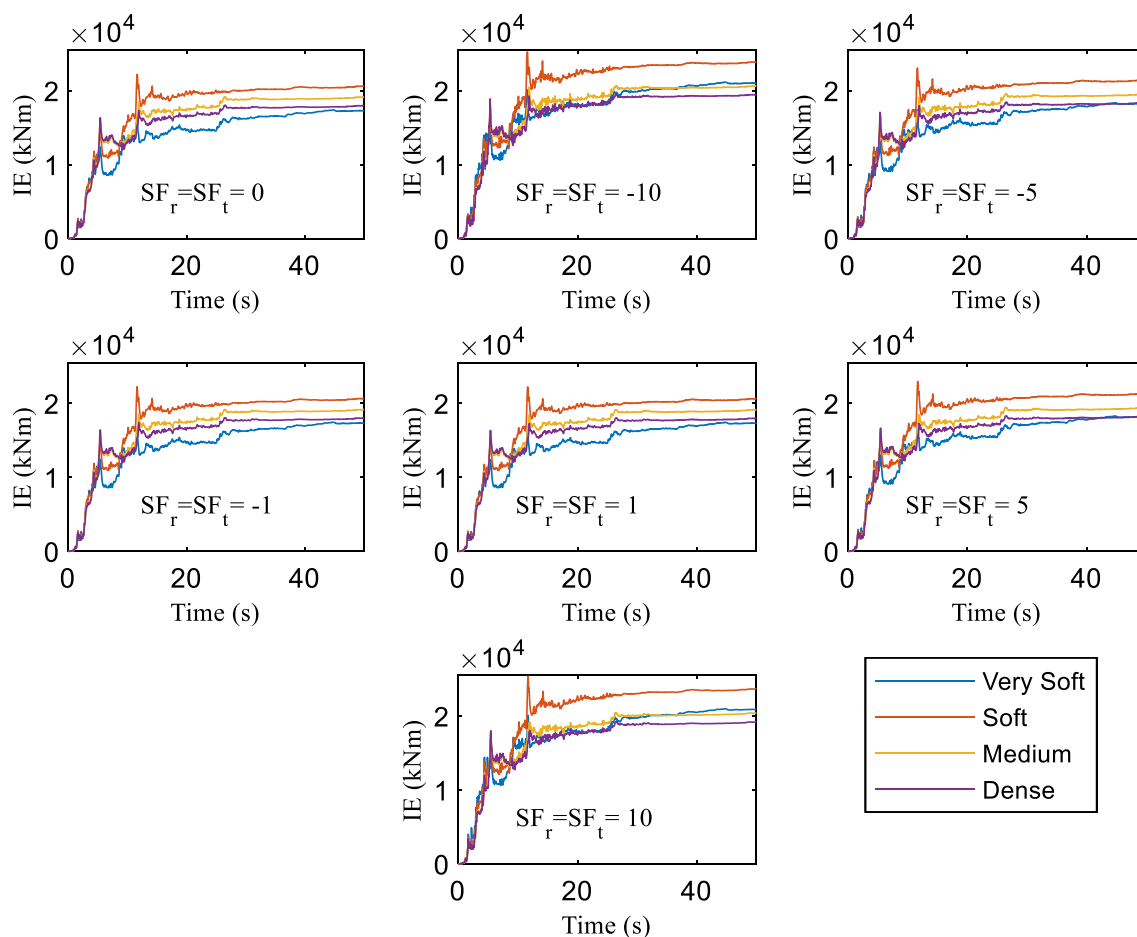
Fig. 15 Seismic input energy for different soil types with varying scale factor coefficients

the structural response parameters, especially when the SFs are higher. It is worth noting that these findings on spectral accelerations are based on the historical earthquake record and model building utilized in the study. The behavior of structures and soil may vary in different building types and ground movements with varying frequency contents.

The isolation effect (ISE) has been seen in the max. FAs and the input energy evaluation indexes when soil shear velocity is less than 100 m/s. This circumstance can be explained as there is no adequate rigid connection between the foundation and the very soft soil which will be able to transfer the

earthquake input excitations fully from the soil through the structure. Therefore, the earthquake excitations are partially dissipated or disported from the structure instead of fully transferring throughout it.

Lastly, it should be mentioned that it is necessary to take rotational components into account to reach more accurate results especially if the foundation is laid on the soil type having a shear velocity of less than 100 m/s.

For future studies, it is recommended to investigate the effects of the rotational component of earthquakes in dynamic analysis for a range of structures , such as bridges, high-rise

Table 7 Seismic input energy for varying scale factor coefficients in dense, medium, soft, and very soft soil

Dense	SF$_r$							
		− 10	− 5	− 1	0	1	5	10
SF$_t$	− 10	19537.74	18876.89	18634.19	18612.87	18606.35	18731.24	19230.92
	− 5	19100.00	18441.16	18199.9	18178.57	18172.06	18297.79	18797.68
	− 1	18959.65	18301.45	18060.66	18039.33	18032.82	18158.83	18658.79
	0				18033.44			
	1	18959.43	18301.23	18060.43	18039.11	18032.6	18158.61	18658.57
	5	19098.88	18440.04	18198.79	18177.47	18170.95	18296.7	18796.6
	10	19535.51	18874.66	18631.98	18610.66	18604.14	18729.05	19228.75
Medium	SF$_r$							
		− 10	− 5	− 1	0	1	5	10
SF$_t$	− 10	20664.55	19996.27	19758.64	19738.72	19734.79	19897.18	20467.83
	− 5	20224.45	19555.05	19317.46	19297.72	19293.45	19454.59	20025.2
	− 1	20083.36	19414.5	19177.27	19157.53	19153.27	19312.72	19883.32
	0				19151.6			
	1	20083.14	19414.29	19177.06	19157.32	19153.05	19312.52	19883.12
	5	20223.37	19553.98	19316.4	19296.66	19292.39	19453.58	20024.21
	10	20662.4	19994.22	19756.59	19736.67	19732.78	19895.17	20465.83
Soft	SF$_r$							
		− 10	− 5	− 1	0	1	5	10
SF$_t$	− 10	25240.74	23340.99	22,659.44	22618.41	22656.14	23310.42	25401.54
	− 5	24956.70	23048.12	22350.9	22302.36	22328.79	22,960.65	25000.85
	− 1	24865.39	22953.98	22251.74	22203.2	22223.6	22848.3	24872.23
	0				22198.92			
	1	24865.05	22953.62	22251.38	22202.85	22223.25	22847.95	24871.89
	5	24954.96	23046.35	22349.12	22300.59	22327.01	22958.88	24999.15
	10	25237.25	23337.46	22655.89	22614.85	22652.59	23306.89	25398.14
Very soft	SF$_r$							
		− 10	− 5	− 1	0	1	5	10
SF$_t$	− 10	21159.79	18734.14	17938.46	17898.54	17922.22	18652.92	20997.35
	− 5	20791.20	18365.56	17569.88	17529.96	17553.64	18284.34	20628.78
	− 1	20671.99	18246.35	17450.67	17410.75	17434.43	18165.13	20509.58
	0				17405.35			
	1	20670.93	18245.3	17449.62	17409.7	17433.38	18164.08	20508.52
	5	20785.94	18360.3	17564.62	17524.7	17548.38	18279.07	20623.52
	10	21149.26	18723.61	17927.94	17888.01	17911.69	18642.39	20986.82

buildings (concrete or steel), and historical masonry buildings. Additionally, estimating the spectral curve can be studied by taking into account the rotational component of earthquakes in regions prone to seismic activity.

Appendix 1: Modal Analysis of the Benchmark Building with Soil–structure Interaction

See Tables 8, 9, 10, 11, 12

Table 8 The first fifteen modal properties of the Benchmark building with fixed-based condition

Mode no	Period	U_x	U_y	U_z	SumU_x	SumU_y	SumU_z	R_x	R_y	R_z	SumR_x	SumR_y	SumR_z
1	2.408	**0.793**	0.034	0.000	0.793	0.034	0.000	0.003	**0.071**	0.000	0.003	0.071	0.000
2	2.397	0.034	**0.788**	0.000	0.827	0.822	0.000	**0.073**	0.003	0.000	0.076	0.074	0.000
3	1.705	0.000	0.000	0.000	0.827	0.822	0.000	0.000	0.000	**0.826**	0.076	0.074	**0.826**
4	0.849	0.082	0.000	0.000	0.909	0.822	0.000	0.000	**0.226**	0.000	0.076	**0.300**	0.826
5	0.823	0.000	0.083	0.000	0.909	0.906	0.000	**0.225**	0.000	0.000	**0.301**	0.300	0.826
6	0.617	0.000	0.000	0.000	0.909	0.906	0.000	0.000	0.000	0.083	0.301	0.300	0.909
7	0.488	0.026	0.000	0.000	0.935	0.906	0.000	0.000	0.033	0.000	0.301	0.333	0.909
8	0.465	0.000	0.027	0.000	0.935	0.932	0.000	0.030	0.000	0.000	0.331	0.333	0.909
9	0.357	0.000	0.000	0.000	0.935	0.932	0.000	0.000	0.000	0.026	0.331	0.333	0.935
10	0.324	0.012	0.000	0.000	0.947	0.932	0.000	0.000	0.024	0.000	0.331	0.356	0.935
11	0.303	0.000	0.014	0.000	0.947	0.946	0.000	0.027	0.000	0.000	0.357	0.356	0.935
12	0.238	0.009	0.000	0.000	0.956	0.946	0.000	0.000	0.013	0.000	0.357	0.370	0.935
13	0.237	0.000	0.000	0.000	0.956	0.946	0.000	0.000	0.000	0.013	0.357	0.370	0.947
14	0.221	0.000	0.010	0.000	0.956	0.957	0.000	0.013	0.000	0.000	0.370	0.370	0.947
15	0.217	0.000	0.000	**0.660**	0.956	0.957	**0.660**	0.000	0.000	0.000	**0.370**	**0.370**	**0.947**

U_x, U_y, U_z = Modal mass participation ratio in the lateral (x-,y-,z-) directions. R_x, R_y, R_z = Modal mass participation ratio in the rocking (rotation around x-,y-) and torsional (rotation around z-) directions, in order
SumU_x, SumU_y, SumU_z; SumR_x, SumR_y, SumR_z = Sum of modal mass participation ratio in the relevant directions

Table 9 The first fifteen modal properties of the Benchmark building placed on dense soil

Mode no	Period	U_x	U_y	U_z	SumU_x	SumU_y	SumU_z	R_x	R_y	R_z	SumR_x	SumR_y	SumR_z
1	2.632	0.001	**0.829**	0.000	0.001	0.829	0.000	**0.072**	0.000	0.000	0.072	0.000	0.000
2	2.628	**0.832**	0.001	0.000	0.832	0.829	0.000	0.000	**0.071**	0.000	0.072	0.071	0.000
3	1.860	0.000	0.000	0.000	0.832	0.829	0.000	0.000	0.000	**0.833**	0.072	0.071	**0.833**
4	0.911	0.081	0.000	0.000	0.914	0.829	0.000	0.000	**0.233**	0.000	0.072	**0.304**	0.833
5	0.891	0.000	0.082	0.000	0.914	0.912	0.000	**0.234**	0.000	0.000	**0.306**	0.304	0.833
6	0.661	0.000	0.000	0.000	0.914	0.912	0.000	0.000	0.000	0.081	0.306	0.304	0.914
7	0.519	0.025	0.000	0.000	0.939	0.912	0.000	0.000	0.033	0.000	0.306	0.338	0.914
8	0.499	0.000	0.026	0.000	0.939	0.938	0.000	0.030	0.000	0.000	0.336	0.338	0.914
9	0.380	0.000	0.000	0.000	0.939	0.938	0.000	0.000	0.000	0.026	0.336	0.338	0.940
10	0.342	0.013	0.000	0.000	0.952	0.938	0.000	0.000	0.025	0.000	0.336	0.362	0.940
11	0.324	0.000	0.014	0.000	0.952	0.952	0.000	0.028	0.000	0.000	0.364	0.362	0.940
12	0.251	0.010	0.000	0.000	0.962	0.952	0.000	0.000	0.015	0.000	0.364	0.377	0.940
13	0.250	0.000	0.000	0.000	0.962	0.952	0.000	0.000	0.000	0.013	0.364	0.377	0.953
14	0.231	0.000	0.011	0.000	0.962	0.963	0.000	0.013	0.000	0.000	0.378	0.377	0.953
15	0.228	0.000	0.000	**0.682**	0.962	0.963	**0.682**	0.000	0.000	0.000	**0.378**	**0.377**	**0.953**

U_x, U_y, U_z = Modal mass participation ratio in the lateral (x-,y-,z-) directions. R_x, R_y, R_z = Modal mass participation ratio in the rocking (rotation around x-,y-) and torsional (rotation around z-) directions, in order
SumU_x, SumU_y, SumU_z; SumR_x, SumR_y, SumR_z = Sum of modal mass participation ratio in the relevant directions

Table 10 The first fifteen modal properties of the Benchmark building placed on medium soil

Mode no	Period	U_x	U_y	U_z	SumU_x	SumU_y	SumU_z	R_x	R_y	R_z	SumR_x	SumR_y	SumR_z
1	2.680	0.000	**0.839**	0.000	0.000	0.839	0.000	**0.069**	0.000	0.000	0.069	0.000	0.000
2	2.666	**0.840**	0.000	0.000	0.840	0.839	0.000	0.000	**0.068**	0.000	0.069	0.068	0.000
3	1.890	0.000	0.000	0.000	0.840	0.839	0.000	0.000	0.000	**0.842**	0.069	0.068	**0.842**
4	0.920	0.080	0.000	0.000	0.921	0.839	0.000	0.000	**0.243**	0.000	0.069	**0.311**	0.842
5	0.902	0.000	0.080	0.000	0.921	0.919	0.000	**0.245**	0.000	0.000	**0.313**	0.311	0.842
6	0.668	0.000	0.000	0.000	0.921	0.919	0.000	0.000	0.000	0.080	0.313	0.311	0.922
7	0.524	0.025	0.000	0.000	0.945	0.919	0.000	0.000	0.034	0.000	0.313	0.345	0.922
8	0.505	0.000	0.025	0.000	0.945	0.945	0.000	0.031	0.000	0.000	0.344	0.345	0.922
9	0.383	0.000	0.000	0.000	0.945	0.945	0.000	0.000	0.000	0.025	0.344	0.345	0.947
10	0.345	0.013	0.000	0.000	0.958	0.945	0.000	0.000	0.026	0.000	0.344	0.371	0.947
11	0.327	0.000	0.014	0.000	0.958	0.959	0.000	0.030	0.000	0.000	0.374	0.371	0.947
12	0.254	0.011	0.000	0.000	0.969	0.959	0.000	0.000	0.016	0.000	0.374	0.387	0.947
13	0.253	0.000	0.000	0.000	0.969	0.959	0.000	0.000	0.000	0.013	0.374	0.387	0.960
14	0.240	0.000	0.000	**0.710**	0.969	0.959	**0.711**	0.000	0.000	0.000	0.374	0.387	0.960
15	0.234	0.000	0.011	0.000	0.969	0.970	**0.711**	0.010	0.000	0.000	**0.384**	**0.387**	**0.960**

U_x, U_y, U_z = Modal mass participation ratio in the lateral (x-,y-,z-) directions. R_x, R_y, R_z = Modal mass participation ratio in the rocking (rotation around x-,y-) and torsional (rotation around z-) directions, in order
SumU_x, SumU_y, SumU_z; SumR_x, SumR_y, SumR_z = Sum of modal mass participation ratio in the relevant directions

Table 11 The first fifteen modal properties of the Benchmark building placed on soft soil

Mode no	Period	U_x	U_y	U_z	SumU_x	SumU_y	SumU_z	R_x	R_y	R_z	SumR_x	SumR_y	SumR_z
1	2.923	0.000	**0.873**	0.000	0.000	0.873	0.000	**0.056**	0.000	0.000	0.056	0.000	0.000
2	2.883	**0.871**	0.000	0.000	0.872	0.873	0.000	0.000	**0.057**	0.000	0.056	0.057	0.000
3	2.030	0.000	0.000	0.000	0.872	0.873	0.000	0.000	0.000	**0.878**	0.056	0.057	**0.878**
4	0.963	0.073	0.000	0.000	0.945	0.873	0.000	0.000	**0.289**	0.000	0.056	**0.346**	0.878
5	0.951	0.000	0.072	0.000	0.945	0.945	0.000	**0.294**	0.000	0.000	**0.350**	0.346	0.878
6	0.699	0.000	0.000	0.000	0.945	0.945	0.000	0.000	0.000	0.070	0.350	0.346	0.947
7	0.543	0.021	0.000	0.000	0.966	0.945	0.000	0.000	0.035	0.000	0.350	0.380	0.947
8	0.525	0.000	0.020	0.000	0.966	0.965	0.000	0.030	0.000	0.000	0.380	0.380	0.947
9	0.398	0.000	0.000	0.000	0.966	0.965	0.000	0.000	0.000	0.020	0.380	0.380	0.968
10	0.370	0.000	0.000	**0.803**	0.966	0.965	**0.803**	0.000	0.000	0.000	0.380	0.380	0.968
11	0.359	0.012	0.000	0.000	0.978	0.965	0.803	0.000	0.053	0.000	0.380	0.434	0.968
12	0.344	0.000	0.001	0.000	0.978	0.966	0.803	0.036	0.344	0.000	0.416	0.777	0.968
13	0.343	0.000	0.005	0.000	0.978	0.971	0.803	0.320	0.042	0.000	0.736	0.819	0.968
14	0.340	0.000	0.007	0.000	0.978	0.977	0.803	0.080	0.001	0.000	0.816	0.819	0.968
15	0.316	0.000	0.000	0.000	0.978	0.977	**0.803**	0.000	0.000	0.000	**0.816**	**0.819**	**0.968**

U_x, U_y, U_z = Modal mass participation ratio in the lateral (x-,y-,z-) directions. R_x, R_y, R_z = Modal mass participation ratio in the rocking (rotation around x-,y-) and torsional (rotation around z-) directions, in order
SumU_x, SumU_y, SumU_z; SumR_x, SumR_y, SumR_z = Sum of modal mass participation ratio in the relevant directions

Table 12 The first fifteen modal properties of the Benchmark building placed on very soft soil

Mode no.	Period	U_x	U_y	U_z	SumU_x	SumU_y	SumU_z	R_x	R_y	R_z	SumR_x	SumR_y	SumR_z
1	3.205	**0.005**	**0.880**	0.000	0.005	0.880	0.000	**0.060**	0.000	0.000	0.060	0.000	0.000
2	3.182	**0.882**	**0.005**	0.000	0.887	0.886	0.000	0.000	**0.060**	0.000	0.061	0.060	0.000
3	2.159	0.000	0.000	0.000	0.887	0.886	0.000	0.000	0.000	**0.902**	0.061	0.060	**0.902**
4	1.008	0.073	0.000	0.000	0.960	0.886	0.000	0.000	**0.368**	0.000	0.061	**0.428**	0.902
5	0.993	0.000	0.072	0.000	0.960	0.958	0.000	**0.373**	0.000	0.000	**0.433**	0.428	0.902
6	0.723	0.000	0.000	0.001	0.960	0.958	0.001	0.000	0.000	0.000	0.061	0.433	0.428	0.963
7	0.656	0.000	0.000	**0.891**	0.960	0.958	**0.892**	0.000	0.000	0.000	0.433	0.428	0.963
8	0.566	0.002	0.000	0.000	0.962	0.958	0.892	0.001	0.464	0.000	0.434	0.892	0.963
9	0.562	0.001	0.000	0.000	0.962	0.958	0.892	0.399	0.000	0.000	0.833	0.893	0.963
10	0.558	0.015	0.000	0.000	0.978	0.958	0.892	0.017	0.002	0.000	0.849	0.895	0.963
11	0.538	0.000	0.018	0.000	0.978	0.975	0.892	0.043	0.000	0.000	0.892	0.895	0.963
12	0.476	0.000	0.000	0.000	0.978	0.975	0.892	0.000	0.000	0.000	0.892	0.895	0.963
13	0.449	0.000	0.000	0.090	0.978	0.975	0.983	0.000	0.000	0.000	0.892	0.895	0.963
14	0.433	0.000	0.000	0.005	0.978	0.975	0.987	0.000	0.000	0.000	0.892	0.895	0.963
15	0.316	0.000	0.000	0.000	0.978	0.977	**0.803**	0.000	0.000	0.000	**0.816**	**0.819**	**0.968**

U_x, U_y, U_z = Modal mass participation ratio in the lateral (x-,y-,z-) directions. R_x, R_y, R_z = Modal mass participation ratio in the rocking (rotation around x-,y-) and torsional (rotation around z-) directions, in order

SumU_x, SumU_y, SumU_z; SumR_x, SumR_y, SumR_z = Sum of modal mass participation ratio in the relevant directions

References

1. Eurocode 8-Part 6. Eurocode 8: Design of structures for earthquake resistance - Part 6: Towers, masts and chimneys SS-EN 1998-6:2005 - Swedish Institute for Standards, SIS (2005)

2. American Society of Civil Engineers: Minimum Design Loads and Associated Criteria for Buildings and Other Structures. American Society of Civil Engineers, Reston (2022) https://doi.org/10.1061/9780784415788

3. Afet ve Acil Durum Yönetimi Başkanlığı. Deprem Etkisi Altında Binaların Tasarımı İçin Esaslar (2018)

4. Akyürek, O.: Depremin dönme bileşenlerinin yapıların dinamik davranışları üzerindeki etkisi. In: 4th International Eurasian Conference on Science, Engineering and Technology (EurasianSciEnTech 2022), pp. 259–66 (2022)

5. Aksoylu, C.; Mobark, A.; Hakan Arslan, M.; Hakkı, E.İ: A comparative study on ASCE 7–16, TBEC-2018 and TEC-2007 for reinforced concrete buildings. Rev. Constr. **19**, 282–305 (2020). https://doi.org/10.7764/rdlc.19.2.282-305

6. Güéguen, P.; Astorga, A.: The torsional response of civil engineering structures during earthquake from an observational point of view. Sensors (Switzerland) **21**, 1–21 (2021). https://doi.org/10.3390/s21020342

7. Basu, D.; Whittaker, A.S.; Constantinou, M.C.: Estimating rotational components of ground motion using data recorded at a single station. J. Eng. Mech. **138**, 1141–1156 (2012). https://doi.org/10.1061/(asce)em.1943-7889.0000408

8. Maranò, S.; Fäh, D.: Processing of translational and rotational motions of surface waves: performance analysis and applications to single sensor and to array measurements. Geophys. J. Int. **196**, 317–339 (2013). https://doi.org/10.1093/gji/ggt187

9. Sollberger, D.; Igel, H.; Schmelzbach, C.; Edme, P.; van Manen, D.J.; Bernauer, F., et al.: Seismological processing of six degree-of-freedom ground-motion data. Sensors (Switzerland) **20**, 1–32 (2020). https://doi.org/10.3390/s20236904

10. Zembaty, Z.; Bernauer, F.; Igel, H.; Schreiber, K.U.: Rotation rate sensors and their applications. Sensors (2021). https://doi.org/10.3390/s21165344

11. Basu, D.; Whittaker, A.S.; Constantinou, M.C.: Characterizing the Rotational Components of Earthquake Ground Motion. State University of New York, Buffalo (2012)

12. Takeo, M.: Rotational motions observed during an earthquake swarm in April 1998 offshore Ito, Japan. Bull. Seismol. Soc. Am. **99**, 1457–1467 (1998). https://doi.org/10.1785/0120080173

13. Teisseyre, R.; Suchcicki, J.; Teisseyre, K.P.; Wiszniowski, J.; Palangio, P.: Seismic rotation waves: basic elements of theory and recording. Ann. Geophys. **46**, 671–685 (2003)

14. Lee, W.; Igel, H.; Trifunac, M.: Recent advances in rotational seismology. Seismol. Res. Lett. **80**, 479–490 (2009). https://doi.org/10.1785/gssrl.80.3.479

15. Lee, W.H.K.; Çelebi, M.; Todorovska, M.I.; Igel, H.: Introduction to the special issue on rotational seismology and engineering applications. Bull. Seismol. Soc. Am. **99**, 945–957 (2009). https://doi.org/10.1785/0120080344

16. Igel, H.; Bernauer, M.: Seismology, rotational, complexity. In: Meyers, R.A. (Ed.) Encyclopedia of Complexity and Systems Science, pp. 1–26. Springer Berlin Heidelberg, Berlin (2015). https://doi.org/10.1007/978-3-642-27737-5_608-1

17. Liu, C.; Huang, B.; Lin, C.: Observing rotational and translational ground motions at the HGSD station in Taiwan from 2007 to 2008. Bull. Seismol. Soc. Am. **99**, 1228–1236 (2009). https://doi.org/10.1785/0120080156

18. Wassermann, J.; Lehndorfer, S.; Igel, H.; Schreiber, U.: Performance test of a commercial rotational motions sensor. Bull. Seismol. Soc. Am. **99**, 1449–1456 (2009)

19. Whittaker, A.S.; Basu, D.; Asce, M.; Constantinou, M.C.: Estimating rotational components of ground motion using data recorded at a single station. J. Eng. Mech. **138**, 1141–1156 (2012). https://doi.org/10.1061/(ASCE)EM.1943-7889.0000408

20. Niazi, M.: Inferred displacements, velocities and rotations of a long rigid foundation located at El Centro differential array site during the 1979 imperial valley, California, earthquake. Earthq. Eng. Struct. Dyn. **14**, 531–542 (1986). https://doi.org/10.1002/EQE.4290140404

21. Spudich, P.; Fletcher, J.: Observation and prediction of dynamic ground strains, tilts, and torsions caused by the M_w 6.0 2004 Parkfield, California, earthquake and aftershocks, derived from UPSAR array observations. Bull. Seismol. Soc. Am. **98**, 1898–1914 (2008). https://doi.org/10.1785/0120100138

22. Basu, D.; Whittaker, A.S.; Constantinou, M.C.: Extracting rotational components of earthquake ground motion using data recorded at multiple stations. Earthq. Eng. Struct. Dyn. **42**, 451–468 (2013). https://doi.org/10.1002/eqe.2233

23. Basu, D.; Whittaker, A.; Constantinou, M.: Characterizing rotational components of earthquake ground motion using a surface distribution method and response of sample structures. Eng. Struct. **99**, 685–707 (2015)

24. Jomen, T.; Murata, A.; Kitaura, M.; Miyajima, M.: Rocking component of earthquake induced by horizontal motion in irregular form foundation. In: 3th World Conference on Earthquake Engineering, pp. 1–7 (2004)

25. Vaseva, E.; Blagov, D.; Bonev, Z.; Vaseva, E.; Blagov, D.; Mladenov, K.: Seismic design of slender structures including rotational components of the ground acceleration–Eurocode 8 approach. In: 14th European Conference on Earthquake Engineering, pp. 1–8 (2010)

26. Pnevmatikos, N.; Konstandakopoulou, F.; Papagiannopoulos, G.; Hatzigeorgiou, G.; Papavasileiou, G.: Influence of earthquake rotational components on the seismic safety of steel structures. Vibration **3**, 42–50 (2020). https://doi.org/10.3390/vibration3010005

27. Federal Emergency Management Agency (FEMA): FEMA 355F—state of the art report on performance prediction and evaluation of steel moment-frame buildings. Fema-355F **1**, 1–367 (2000)

28. Ohtori, Y.; Christenson, R.E.; Spencer, B.F.; Dyke, S.J.: Benchmark control problems for seismically excited nonlinear buildings. J. Eng. Mech. **130**, 366–385 (2004). https://doi.org/10.1061/(ASCE)0733-9399(2004)130:4(366)

29. Computers and Structures Inc: SAP2000 integrated software for structural analysis and design. Computers and Structures Inc, Walnut Creek (2020)

30. MathWorks MATLAB. SIMULINK for Technical Computing. Available on https://www.mathworks.com/2023 (2022)

31. Shehata, O.E.; Farid, A.F.; Rashed, Y.F.: A suggested dynamic soil–structure interaction analysis. J. Eng. Appl. Sci. (2023). https://doi.org/10.1186/s44147-023-00237-1

32. Kant, L.; Samanta, A.: Nonlinear analysis of building structures resting on soft soil considering soil–structure interaction and structure–soil–structure interaction. J. Inst. Eng. India Ser. A (2024). https://doi.org/10.1007/s40030-024-00788-3

33. Givens, M.J.: Dynamic Soil–Structure Interaction of Instrumented Buildings and Test Structures. University of California, Los Angeles (2013)

34. Jarernprasert, S.; Bazan-Zurita, E.; Bielak, J.: Seismic soil–structure interaction response of inelastic structures. Soil Dyn. Earthq. Eng. **47**, 132–143 (2013). https://doi.org/10.1016/j.soildyn.2012.08.008

35. Yanik, A.: Seismic control performance indices for magnetorheological dampers considering simple soil–structure interaction. Soil Dyn. Earthq. Eng. (2020). https://doi.org/10.1016/j.soildyn.2019.105964

36. Hosseini Lavassani, S.H.; Ebadijalal, M.; Shahrouzi, M.; Gharehbaghi, V.; Noroozinejad Farsangi, E.; Yang, T.Y.: Interpretation of simultaneously optimized fuzzy controller and active tuned mass damper parameters under pulse-type ground motions. Eng. Struct. (2022). https://doi.org/10.1016/j.engstruct.2022.114286

37. Yanik, A.; Ulus, Y.: Soil–structure interaction consideration for base isolated structures under earthquake excitation. Buildings (2023). https://doi.org/10.3390/buildings13040915

38. Bapir, B.; Abrahamczyk, L.; Wichtmann, T.; Prada-Sarmiento, L.F.: Soil-structure interaction: a state-of-the-art review of modeling techniques and studies on seismic response of building structures. Front. Built. Environ. (2023). https://doi.org/10.3389/fbuil.2023.1120351

39. Wolf, J.P.: Simple physical models for foundation dynamics. In: International Conferences on Recent Advances in Geotechnical Earthquake Engineering and Soil Dynamics, vol. II, pp. 943–984 (1995)

40. PEER Ground Motion Database - PEER Center. PEER Ground Motion Database - PEER Center n.d. https://ngawest2.berkeley.edu/. Accessed 18 May 2022

41. Abdel Raheem, S.E.; Ahmed, M.M.M.; Ahmed, M.M.; Abdelshafy, A.G.A.: Evaluation of plan configuration irregularity effects on seismic response demands of L-shaped MRF buildings. Bull. Earthq. Eng. **16**, 3845–3869 (2018). https://doi.org/10.1007/s10518-018-0319-7

42. López Jiménez, G.A.; Dias, D.: Dynamic soil-structure interaction effects in buildings founded on vertical reinforcement elements. CivilEng **3**, 573–593 (2022). https://doi.org/10.3390/civileng3030034

43. Ucar, T.: Computing input energy response of MDOF systems to actual ground motions based on modal contributions. Earthq. Struct. **18**, 263–273 (2020). https://doi.org/10.12989/EAS.2020.18.2.263